

A New Noninvasively Adjustable Glaucoma Drainage Device

THÈSE N° 6295 (2014)

PRÉSENTÉE LE 18 SEPTEMBRE 2014

À LA FACULTÉ DES SCIENCES DE LA VIE

LABORATOIRE D'HÉMODYNAMIQUE ET DE TECHNOLOGIE CARDIOVASCULAIRE (SV/STI)

PROGRAMME DOCTORAL EN BIOTECHNOLOGIE ET GÉNIE BIOLOGIQUE

ÉCOLE POLYTECHNIQUE FÉDÉRALE DE LAUSANNE

POUR L'OBTENTION DU GRADE DE DOCTEUR ÈS SCIENCES

PAR

Adan VILLAMARIN

acceptée sur proposition du jury:

Prof. J. McKinney, président du jury
Prof. N. Stergiopoulos, directeur de thèse
Prof. A. Bron, rapporteur
Prof. A. Mermoud, rapporteur
Prof. Ph. Renaud, rapporteur



ÉCOLE POLYTECHNIQUE
FÉDÉRALE DE LAUSANNE

Suisse
2014

Para mi Rosa

Acknowledgments

Because without a proper environment, support and guidance such a work would not have been possible, I therefore take this opportunity to express my gratitude to all the people that supported me during my education and work.

Firstly, I would like to express my deepest gratitude to Professor Nikos Stergiopoulos. At the end of my Master's studies, you very kindly offered to me this great opportunity. You constantly provided invaluable support, enthusiasm, help, new ideas, and motivation to guide me through this work.

I deeply thank Dr. Sylvain Roy for his invaluable help at each step of my thesis. His experience in ophthalmology, his intellectual support and his expertise in methodological aspects of scientific work, were priceless for the success of this work. I am equally grateful to Stéphane Bigler for his endless help in designing and conceiving new parts. Your expertise in manufacturing and machining as well as your engineering skills were an endless source of inspiration

For his constant help and kind advice, I would like to especially thank Professor André Mermoud. Your knowledge and passion for the field was inestimable for the success of the thesis.

As member of the jury I would like to thank Prof. Renaud and Prof. Bron for their participation and Prof. McKinney for having accepted to be the jury president. I highly appreciated their valuable comments and feedback.

It has been a true pleasure working in LHTC and I am indebted to all the members of the group for their great companionship and for all the unforgettable moments: Rodrigo, Fabiana, Orestis, Thiresia, Michel, Bram, Tamina, Christian, Lydia. I also would like to acknowledge the students who have contributed to various aspects of this work through their semester and diploma projects (in order of appearance): Mustapha, Reda, Andreas, Benjamin, Raphaël, Laura, Soraya, Valérie, Nick and Efstathios.

I would like to express my deepest gratitude to my family for their constant help and motivation through the entire duration of the thesis. Finally, I especially want to thank Katia. You brought me affection, constantly helped me to get through the hard times and encouraged me over the years. This thesis was possible in part thanks to you.

Abstract

Glaucoma is an irreversible disease affecting the eye, leading to progressive loss of vision and eventually to total blindness. It is often related to high intraocular pressure (IOP), which results from increased outflow resistance to aqueous humor. The first line of treatment to stop or slow down the progression of the disease is based on medication, but when this fails one has to resort to invasive methods, such as filtering surgery. Filtering surgery, including drainage implants or aqueous shunts, aims in reducing intraocular pressure by creating an additional outflow conduit to aqueous humor. However, even if filtering surgery is effective in lowering intraocular pressure, it is often associated with several complications that could potentially lead to further damages impairing the sight. The origin of most complications can be traced to a fundamental mechanism: poor flow control. Among others, hypotony (IOP < 5 mmHg) is one of the most frequent complications after glaucoma filtering surgery. Hypotony is a consequence of very low outflow resistance, leading in some severe cases to anterior chamber flattening or choroidal detachment, among others. Consequently, modifications to glaucoma drainage devices and new surgical techniques were developed to minimize the rates of early post-operative hypotony. Unfortunately, these techniques are poorly reproducible and not fully predictable. At present, there are no real alternatives at hand to clearly improve the success rate of filtering surgery outcomes.

In view of the aforementioned problems related to filtering surgery, a new glaucoma drainage device has been developed. This draining implant has the same function like any of the current drainage devices but with the specific additional feature of an adjustable resistor to the aqueous humor egress. The device is non-invasively adjustable allowing for a non-traumatic change of the resistance during the entire post-operative period. In vitro tests realized on enucleated rabbit eyes and in vivo tests on rabbits have shown the efficacy of the implant in reducing the pressure by selectively adjusting the resistor. Biocompatibility tests have also been performed to ensure the safety of the device for human use. The ease of use and the reproducibility of the measurements indicate that the novel implant can be potentially of great utility in filtering surgery, offering great flow control, reducing complications rates and leading to better clinical outcomes.

Keywords

Glaucoma; filtering surgery; aqueous shunt; glaucoma drainage device; aqueous humor.

Résumé

Le glaucome est une maladie irréversible qui affecte l'œil et qui conduit progressivement à une perte de vue voire même à la cécité. Il est souvent associé à une haute pression intraoculaire (PIO), qui résulte d'une augmentation de la résistance à l'écoulement de l'humeur aqueuse. Le premier type de traitement pour stopper ou freiner la progression de cette maladie repose sur des médicaments, mais quant ceux-ci ne sont pas suffisants, il faut envisager des méthodes plus invasives comme la chirurgie filtrante. La chirurgie filtrante, qui inclut l'utilisation d'implants de drainage, a pour but de réduire la PIO en créant une voie d'écoulement additionnel à l'humeur aqueuse. Néanmoins, même si cette méthode est efficace pour réduire la pression intraoculaire, elle est associée à un nombre non négligeable de complications qui peuvent potentiellement conduire à des dommages affectant la vue du patient. L'origine de ces complications a comme dénominateur commun un manque de contrôle dans l'écoulement de l'humeur aqueuse. Parmi d'autres, l'hypotonie ($PIO \leq 5$ mmHg) est l'une des complications les plus fréquentes liée à la chirurgie filtrante. L'hypotonie est due à une résistance d'écoulement trop petite conduisant dans des cas extrêmes au décollement de la choroïde ou à une chambre aplatie, par exemple. Par conséquent plusieurs modifications ont été apportées aux implants de drainage et de nouvelles méthodes ont été développées afin de minimiser le taux d'hypotonie post-opératoire. Malheureusement, ces techniques sont peu reproductibles et peu prévisibles. Actuellement, il n'y a pas de réelle alternative à disposition pour améliorer le taux de succès du devenir d'une chirurgie filtrante.

En relation avec les problèmes liés à la chirurgie filtrante cités ci-dessus, un nouvel implant de drainage pour le glaucome a été développé. Cet implant obéit au même concept que les implants existants actuellement, mais avec l'addition d'une résistance modulable à l'écoulement de l'humeur aqueuse. Ce dispositif est ajustable non invasivement ce qui permet un réglage non traumatique de la résistance à l'écoulement tout au long du suivi du patient. Des tests in vitro réalisés sur des yeux énucléés de lapins ainsi que des tests in vivo sur des lapins, ont montré l'efficacité de l'implant en réduisant la pression de l'œil, en ajustant sélectivement la résistance appropriée. Des tests de biocompatibilités ont également démontré que l'implant est sûr pour une utilisation humaine. La facilité d'emploi ainsi que la reproductibilité des mesures indiquent que ce nouvel implant peut être d'un grand bénéfice pour la chirurgie filtrante, en apportant un contrôle effectif sur l'écoulement de l'humeur aqueuse, réduisant ainsi les complications et permettant de meilleurs résultats cliniques.

Mots clés

Glaucome ; chirurgie filtrante ; implant de drainage ; humeur aqueuse ; pression intraoculaire.

Content

ACKNOWLEDGMENTS	3
ABSTRACT	5
KEYWORDS	5
RÉSUMÉ	7
CONTENT	9
LIST OF FIGURES	11
LIST OF TABLES	12
CHAPTER 1 : INTRODUCTION	13
1.1 MOTIVATION	14
1.2 GLAUCOMA AND AQUEOUS HUMOR	14
1.3 FILTERING SURGERY	15
1.4 GLAUCOMA DRAINAGE DEVICES	17
1.5 HYPOTONY	22
1.6 TUBE-CORNEA TOUCH	23
1.7 HYPERTENSIVE PHASE	24
1.8 REQUIREMENTS FOR NEXT GDD GENERATION	26
1.9 REFERENCES	27
CHAPTERS	31
PAPER 1	31
PAPER 2	31
PAPER 3	32
PAPER 4	33
CHAPTER 2 : 1ST PAPER	35
2.1 INTRODUCTION	37
2.2 MATERIAL AND METHODS	39
2.3 RESULTS	43
2.4 DISCUSSION	50
2.5 CONCLUSION	54
2.6 ACKNOWLEDGEMENTS	56
2.7 REFERENCES	57
CHAPTER 3 : 2ND PAPER	59
3.1 INTRODUCTION	61
3.2 MATERIALS AND METHODS	62
3.3 RESULTS	66
3.4 DISCUSSION	67

3.5	ACKNOWLEDGMENTS	70
3.6	REFERENCES	71
CHAPTER 4	: 3RD PAPER	73
4.1	INTRODUCTION	75
4.2	METHODS AND MATERIALS.....	75
4.3	RESULTS	78
4.4	DISCUSSION	80
4.5	REFERENCES	83
CHAPTER 5	: 4TH PAPER	85
5.1	INTRODUCTION	87
5.2	MATERIALS AND METHODS.....	88
5.3	RESULTS	92
5.4	DISCUSSION	94
5.5	ACKNOWLEDGMENTS	99
5.6	REFERENCES	100
CHAPTER 6	: CONCLUSION	103
PERSPECTIVES		105
CURRICULUM VITAE		106

List of Figures

<i>Figure 1-1</i>	15
<i>Figure 1-2</i>	16
<i>Figure 1-3</i>	17
<i>Figure 1-4</i>	18
<i>Figure 1-5</i>	19
<i>Figure 1-6</i>	19
<i>Figure 1-7</i>	20
<i>Figure 1-8</i>	20
<i>Figure 1-9</i>	21
<i>Figure 1-10</i>	23
<i>Figure 2-1</i>	40
<i>Figure 2-2</i>	44
<i>Figure 2-3</i>	45
<i>Figure 2-4</i>	46
<i>Figure 2-5</i>	47
<i>Figure 2-6</i>	48
<i>Figure 2-7</i>	48
<i>Figure 2-8</i>	49
<i>Figure 2-9</i>	50
<i>Figure 3-1</i>	63
<i>Figure 3-2</i>	63
<i>Figure 3-3</i>	65
<i>Figure 3-4</i>	66
<i>Figure 3-5</i>	67
<i>Figure 4-1</i>	76
<i>Figure 4-2</i>	78
<i>Figure 4-3</i>	79
<i>Figure 4-4</i>	80
<i>Figure 4-5</i>	80
<i>Figure 5-1</i>	90
<i>Figure 5-2</i>	93
<i>Figure 5-3</i>	95

List of Tables

Table 1-1 22
Table 1-2 24
Table 2-1 41
Table 5-1 93

Chapter 1 : Introduction

1.1 Motivation

Glaucoma is one of the leading causes of blindness in the world^{1,2}. It is frequently associated with an elevation of the intraocular pressure (IOP), resulting from an increased resistance to aqueous humor outflow. The increased IOP leads to progressive and permanent damage of the optic nerve and, if left untreated, results eventually in vision loss³. In most of the cases the treatment consists in giving medications that lower IOP. When pharmacological treatments fail, incisional surgery developed to create alternative outflow paths to aqueous humor is indicated. Filtering surgery aims at increasing the aqueous humor outflow, either directly (i.e., trabeculectomy or deep sclerectomy) or through the use of draining implants. Since the inception of aqueous shunts (glaucoma drainage devices, tube implants, tube shunts), their use has increased and these implants are now considered by many to be the first-line surgical intervention for many types of glaucoma⁴. Nonetheless, all filtering surgery methods, including or not pose of drainage tubes, exhibit post-surgical complications, the rate being around 25%⁵. Post-surgical complications can often lead to surgical failures, a significant part of which being attributed to the lack of proper intraocular pressure control over time. This clearly underlines the need for a new generation of drainage implants that could provide a better control of the intraocular pressure (IOP).

1.2 Glaucoma and Aqueous Humor

Intraocular pressure plays a crucial role in the onset and severity of glaucoma. Even if the causes of glaucoma are not yet well understood, elevation of the IOP is one of the main clinical parameters governing the genesis and progression of the disease. IOP refers to the pressure of the aqueous humor (AH), the liquid circulating in the anterior segment of the eyeball. AH is produced at a relatively stable rate by the ciliary body (2 to 3 $\mu\text{l}/\text{minute}$)⁶ and exits the eyeball after passing through different structures such as the trabecular meshwork, the Schlemm's canal and the collector channels (Fig. 1-1). The rate of aqueous humor production and outflow resistance defines the IOP level over time. For subjects without glaucoma, normal IOP values are in the range between 10 and 21 mmHg.

There are several strategies available for the ophthalmologist to lower IOP, depending on the type of glaucoma (geometry, function, disease): a) act on the ciliary body and reduce the rate of production of AH, b) enhance the outflow facility of AH by changing the properties of the draining tissues or c) create an artificial pathway of reduced resistance to AH outflow. Medications are targeting the first two strategies, while surgery addresses the last one. The

fluidics involved in the eye are not well understood and even if some studies have described the behavior of AH flow in the anterior segment in 2D or 3D, little information is found in the literature for flow characteristics following a filtering procedure.

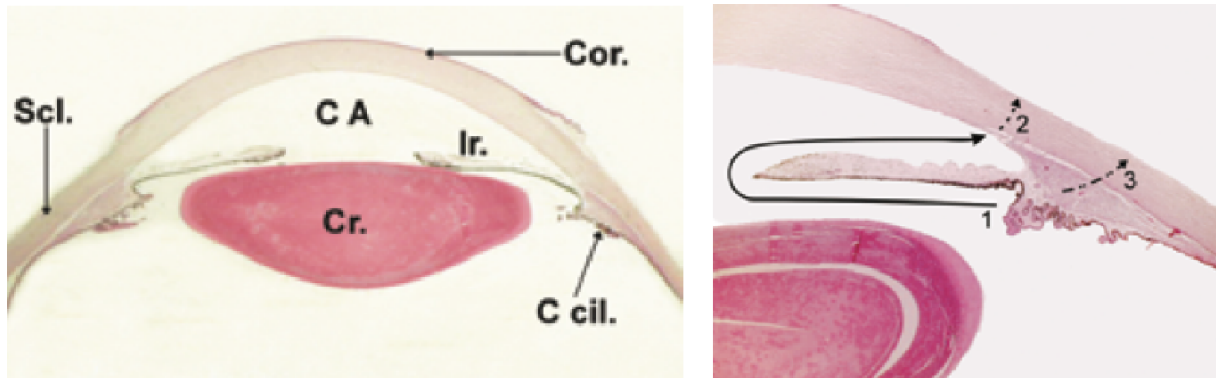


Figure 1-1: : Horizontal slice of anterior chamber passing through the middle of the lens. (left) CA: anterior chamber, Scl: sclera, Cr.: lens, Cor: cornea, C cil: ciliary body, Ir.: iris. (right) aqueous humor route from the ciliary body to and through Schlemm's canal. (images courtesy of Dr. Roy)

1.3 Filtering surgery

1.3.1 Trabeculectomy

At present, several glaucoma-filtering techniques are practiced clinically and most of them have demonstrated their efficacy^{5, 7-10}. Trabeculectomy is the procedure of choice in glaucoma surgery¹¹ (Fig. 1-2). This technique, developed in the late 60s by Cairns¹², shows a fairly good success rate especially when combined with antifibrotic agents such as 5-fluorouracil or mitomycin-C¹³. However, even if trabeculectomy became a standard procedure in glaucoma management¹⁴, it often leads to post-operative complications. Durable hypotony, maculopathy, bleb infections, flat anterior chamber, choroidal detachment, and the lack of predictability in the long-term IOP control, are some of the common serious postoperative complications¹⁵. These complications may result in surgical failure and, in some cases, may lead to irreversible damages.

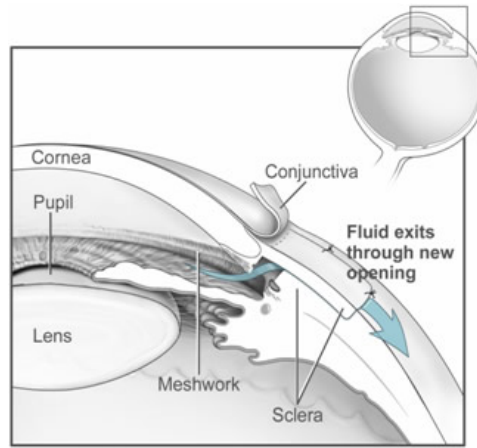


Figure 1-2: Schematic representation of the trabeculectomy procedure and AH flowing through the new openings (<https://doctree.in/knowledgebranch/trabeculectomy>).

1.3.2 Deep sclerectomy

In order to avoid the drawbacks associated with penetrating filtering surgeries (e.g. trabeculectomy) and to improve the predictability of the IOP lowering action, various types of non-penetrating filtering surgeries have been proposed. There are various advantages of the non-penetrating surgery compared to penetrating techniques. Non-invasive procedures increase the predictability of the IOP lowering action and reduce the incidence of complications related to penetrating methods. Fyodorov and Kozlov first described the non-penetrating deep sclerectomy in 1990^{16, 17}. This method consists in removing the main resistance to AH outflow by peeling both the Schlemm's canal trabecular endothelium and the juxtacanalicular trabeculum (Fig. 1-3). This creates a thin membrane at the level of the anterior trabeculum that prevents excessive filtration of AH. In addition, the creation of an intrascleral filtering space, decreases the need for a subconjunctival filtering bleb, allowing the redirection of part of the AH into the subchoroidal space.

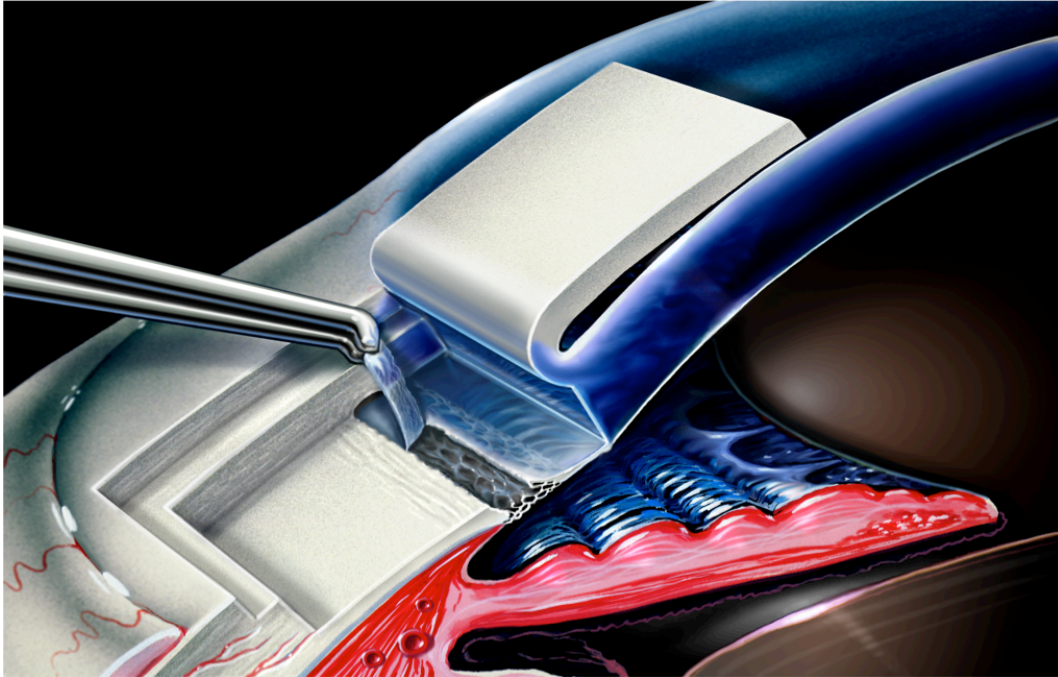


Figure 1-3: Schematic representation of a non-penetrating deep sclerectomy (image courtesy of Dr. Mermoud).

The main advantage of deep sclerectomy resides in the absence of perforation of the anterior chamber, which allows a progressive decrease of the IOP. In some cases, collagen implants are also used to maintain the space under the scleral flap and prevent a collapse of the space. However, even if this technique is efficient in reducing the occurrence of complications related to filtering surgery, the surgical skills required and the level of knowledge of the anterior segment anatomy have limited the adoption of the technique to a rather restricted number of surgeons.

1.4 Glaucoma Drainage Devices

In order to prevent or decrease the rate of complications in filtering surgery or simply to provide other means of drainage when trabeculectomies have failed, various types of glaucoma drainage devices (GDD) have been designed and implemented during the last decades.

1.4.1 History

The idea of creating a hole and to maintain it to treat patients with painful absolute glaucoma came from Rollet and Moreau in 1907 when they decided to implant a horse-hair thread connecting the anterior chamber to the subconjunctival space near the limbus. Later, in 1969, Molteno first hypothesized and confirmed that filtration failure was primarily attributable to subconjunctival fibrosis, with fistula closure occurring as a secondary event. Realizing that

simple anterior GDDs would have little impact on this process, Molteno launched the concept of tube and plate GDDs, in which aqueous fluid is shunted to a plate device designed to maintain patency of a subconjunctival filtration reservoir in the face of continuing subconjunctival fibrosis.

Since the introduction of the first glaucoma drainage device (GDD) by Molteno in 1969¹⁸, little progress has been made in developing new GDD devices with improved and distinctly different features. The design of these implants remained rather similar to the initial concept presented by Molteno; a long tube inserted into the anterior chamber, connected to an external endplate draining the aqueous humor under a filtering bleb. The mechanism of such an implant is relatively simple: the excess of aqueous humor is drained out through the lumen of the tube to reach the episcleral endplate located in the equatorial region of the eyeball. In this area the formation of a fibrous capsule creates a reservoir where the aqueous humor is collected. Some studies have also shown that the size of the endplate would play a role in the efficacy of the aqueous shunt. The dimension of the plate could be a determining factor to ascertain the final IOP¹⁹. Following that principle Molteno has introduced, in 1981, an implant with a double plate enhancing the success rate of the filtering-surgery (success [survival] defined as 6 mmHg < or = final intraocular pressure [IOP] < or = 21 mmHg without additional glaucoma surgery or devastating complication)²⁰. Later, in 1992, Georges Baerveldt introduced a non-valved silicone tube attached to a large barium-impregnated silicone plate with different surface areas²¹ (150, 250, 350 or 500 mm², Fig. 1-4).

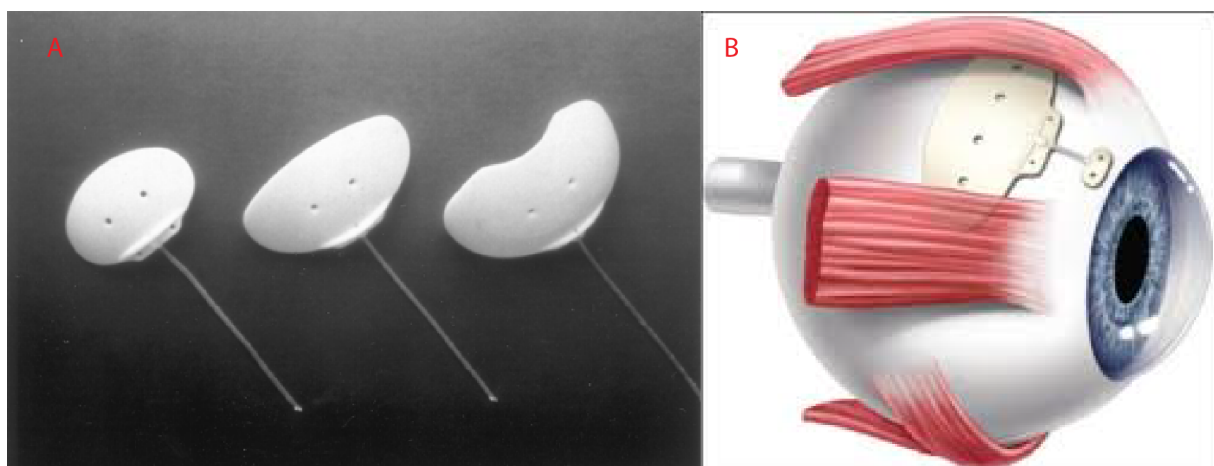


Figure 1-4: a) Baerveldt glaucoma drainage implants are shown in three sizes with surface areas of 250, 350, and 425 mm² (left to right)²² and b) Schematic representation of the placement of a Baerveldt pars-plana.

Molteno and Baerveldt devices do not offer resistance to the outflow of AH and post-operative complications such as hypotony and flat anterior chamber became a regular phenomenon. In that prospect and to minimize the problems related to early post-operative

complications, new non-adjustable valved implants appeared. Theodore Krupin was the first to introduce in 1976 the Krupin® valve. This implant has a slit valve that is designed to be pressure-sensitive and unidirectional. In theory, the valve should open only when IOP reaches 11 mmHg²³. Later, in 1993, Marteen Ahmed introduced the Ahmed® glaucoma valve (New World Medical, Rancho Cucamonga, CA), based on the principle of the Venturi effect with a pressure-sensitive valve that opens at IOPs ≥ 8 mmHg²⁴.



Figure 1-5: Single-plate and double-plate Molteno implants (top row). Krupin slit valve and Ahmed glaucoma valve (middle row). 350 mm² and 250 mm² Baerveldt glaucoma implants (bottom row)⁵⁸.

The aforementioned devices still form the bask of the current GDD market (Fig. 1-5). However, new implants are appearing based on different approaches. This is the case of the Ex-Press® tube (Alcon, Fort Worth, TX, USA), a stainless steel translimbal implant that was originally designed to be implanted under a conjunctival flap but in this position it was unstable and tended to erode through the conjunctiva. It was then placed under a scleral flap in an analogous way to trabeculectomy procedure (Fig. 1-6). This non-valved device demonstrated efficacy in lowering IOP and its easiness for implantation has convinced many surgeons. As it is often compared to an improved trabeculectomy, the Ex-Press shunt is indicated for patients where normally trabeculectomy should be performed.

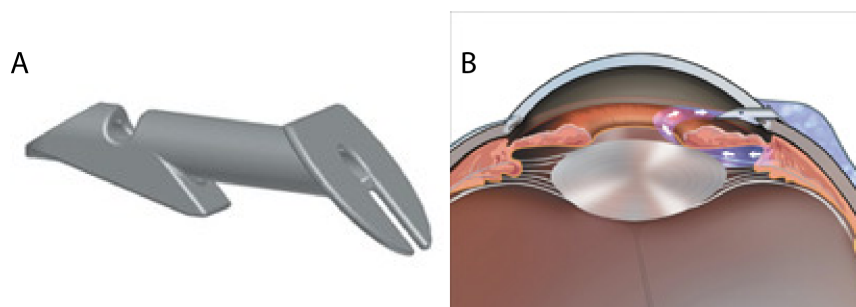


Figure 1-6: a) The Ex-Press P-50 model made of stainless steel and b) how the Ex-Press mini glaucoma shunt works in the eye to divert excess aqueous humor from the anterior chamber to lower intraocular pressure (source Alcon Surgical website).

1.4.2 New and future drainage devices

In this section, a short description of the newest glaucoma drainage devices is given. Most of these devices are still under clinical tests and results need to be published.

The iStent

The iStent (Glaukos, Laguna Hills, CA, USA) is a very small implant made of titanium, which is inserted through the filtering tissue meshwork (Fig. 1-7). The implant creates an opening between the anterior chamber and the Schlemm's canal bypassing the resistive problem and drains the AH out into deeper tissues potentially decreasing IOP.

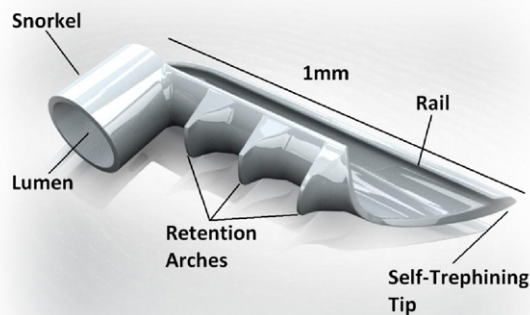


Figure 1-7: The iStent trabecular micro-bypass (source Glaukos website).

The Hydrus Stent

The Hydrus Stent (Ivantis, Irvine, CA, USA) is a promising mini-drainage device that is currently in clinical trial (Fig 1-8). This device is a kind of “intra-canalicular scaffold” made of nitinol. The Hydrus is placed in the Schlemm's canal and creates a bypass through the trabecular meshwork increasing the outflow of AH.



Figure 1-8: The Hydrus Stent (source Ivantis website).

The SolX gold shunt

The SolX gold shunt (SOLX inc., Waltham, MA, USA) is a 24-carat-gold implant designed to increase the uveoscleral outflow from the anterior chamber into the suprachoroidal space through engraved channels (Fig. 1-9).

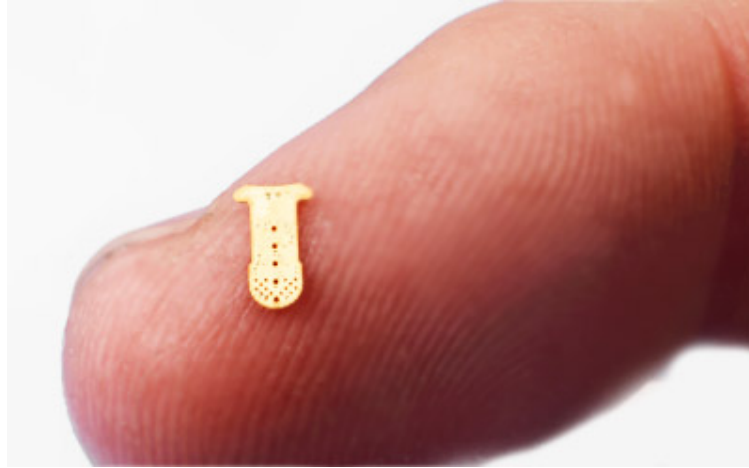


Figure 1-9: The SOLX Gold Suprachoroidal Shunt (*source SOLX website*).

1.4.3 GDD trend

Since 1995 the trend of GDDs in glaucoma surgery is increasing, reaching +184% in 2004 and in comparison, the number of trabeculectomy procedures decreased by 43%²⁵. These data are showing that a growing number of glaucoma specialists are now choosing the glaucoma drainage tubes instead of traditional trabeculectomy as a first option in filtering surgery⁸. Moreover, this tendency is supported by the trabeculectomy versus tube study (TVT)¹¹; five-years results on treatment outcomes and complications where 212 patients were enrolled, including 107 in the tube group (e.g. the Baerveldt 350-mm²), and 105 in the trabeculectomy group. The study demonstrated that the tube group had higher success rate than trabeculectomy combined with mitomycin C. The cumulative probability of failure during these 5 years of follow-up was 29.8% in the tube group and 46.9% in the trabeculectomy group. Additionally, the rate of reoperation for patients enrolled in the tube group was 9% and 29% in the trabeculectomy group. These data demonstrated that glaucoma drainage devices have the potential to increase the success rate of glaucoma filtering surgery.

Table 1-1 gives a summary of most common complications related to trabeculectomy, GDDs and the Ex-Press device, as reported in the literature. Hypotony, corneal issues and hypertensive phases were the most common complications.

Table 1-1: Summary of GDDs and filtering post-operative complications

Glaucoma procedures	Trabeculectomy	Glaucoma Drainage Devices	Ex-Press
Advantages	Most used last decade	Best success rate than Trabeculectomy ^{11, 30-32} Less fibrosis Long-term efficacy ⁹	Surgery similar to trabeculectomy Less post-op visits ⁷ Good IOP reduction ^{7, 26, 27} Reduction of additional medication ^{28, 29}
Complications	No reproducible results Shallow or flat anterior chamber ^{11, 37} Early and Persistent hypotony ⁴⁷ High failure rate ¹¹ Choroidal effusion ⁴⁷ Additional medication	Transient hypotony ^{34, 35} Shallow or flat anterior chamber ^{11, 36} Corneal edema ³¹ Failure in IOP reduction ^{24, 37, 38} Blockage of tube ^{31, 36, 39} Valve membrane adhesion ⁴⁰ High rate of failure ³⁶ Tube touches cornea ⁴¹ Additional surgical steps are required ⁴² Diplopia ^{31, 43, 44} Tube erosion ^{11, 36, 45, 46}	Iris incarceration ⁷ Contact implant-iris ^{26, 33} Early hypotony ^{26, 27} Conjunctival erosion ²⁹ Tube obstruction ^{28, 29} Device rotation ³³

1.5 Hypotony

Early postoperative hypotony is one of the most frequent postoperative complications when performing a glaucoma filtering surgery resulting sometimes to shallow anterior chamber. It is described as a hypotensive state of the eye, which over time, could lead to severe irreversible diseases such as choroidal detachment or hypotony-induced maculopathy. Early hypotony occurs during the first days after placement of the GDD, mainly due to an over filtration of the AH outflow. As a result, IOP decreases to values even lower than 5 mmHg. Often, in the following weeks, the lack of significant outflow resistance does not allow the eye to recover normal IOP levels (i.e., in the range of 10-21 mmHg) and only the formation of a fibrosis capsule around the filtration site can effectively raise the IOP, although the final IOP levels at long-term may vary considerably.

In that prospect efforts were made to prevent hypotony. New implants were designed with flow restrictors or valves. While the incorporation of a valved flow restrictor should theoretically reduce the risk of immediate post-operative hypotony, the reported incidence rates of postoperative hypotony with this kind of GDDs (8-13%) indicate that the valves do not function in vivo as well as expected to do^{48, 49}. Furthermore, leakages around the insertion

point through the sclera or the reduction of aqueous humor production may still result in early hypotony⁵⁰.

For implants such as the Molteno® or the Baerveldt®, which do not possess a valve, surgeons have developed numerous practical, yet not so elegant, solutions to prevent hypotony from occurring: a) an internal tube occlusion using a 4-0 or 5-0 nylon or Prolene suture through the lumen of the tube⁵¹, b) external tube occlusion creating a ligature around the tube with an absorbable or non-absorbable suture (Fig. 1-10A), c) tube obstruction with a collagen plug⁵² (Fig. 1-10B) and d) a two stage procedure where the plate is first attached to the eyeball until formation of fibrosis and then insertion of the tube into the anterior chamber. However, the resistance to aqueous outflow through these tubes depends on the tightness of the suture or the completeness of the occlusion, which vary from surgeon to surgeon depending on the specific procedure. In addition, the rate of hypotony still remains at around 15-16% using either of these techniques⁵⁰. Consequently, while these solutions may be effective in minimizing the occurrence of hypotony they require additional technical steps during surgery, including post-operative management, without guaranteeing an optimal IOP control in all patients.

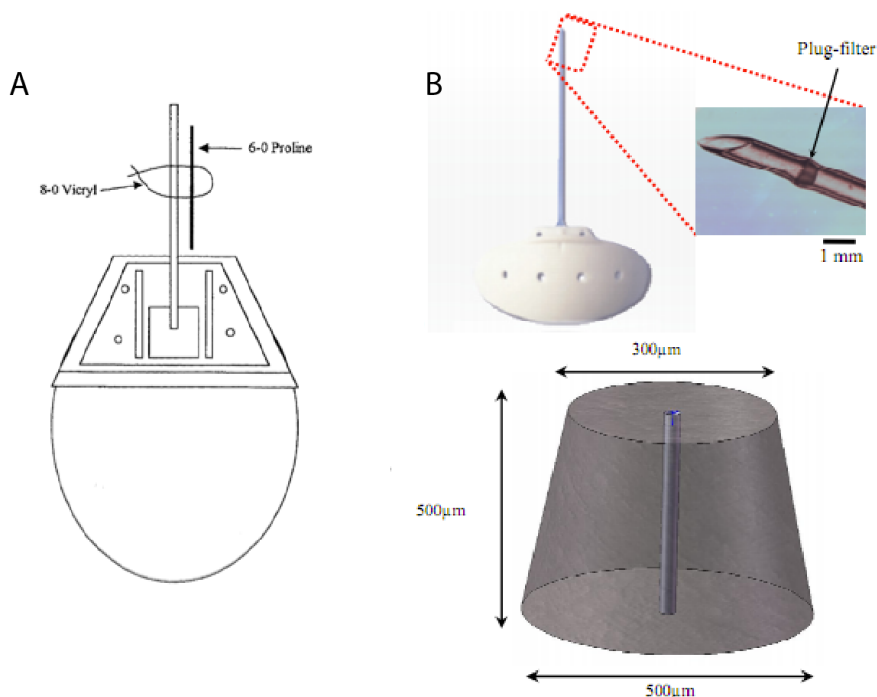


Figure 1-10: Current methods used to prevent early post-operative hypotony. (A) Tube occlusion using an 8-0 Vicryl and a 6-0 Prolene sutures. (B) Collagen plug inserted in the draining tube.

1.6 Tube-cornea touch

Nowadays most of the drainage devices are made of flexible, long and large silicone tubes (~ 0.63 mm external diameter, see Table 1-2). The size and the elasticity of these tubes are

relatively problematic in filtering surgery. Corneal edema and/or corneal graft failure may develop as a consequence the silicone tube touching the corneal endothelial surface. Corneal endothelial damage can occur after tube-endothelial contact during blinking, eye movement or eye rubbing. This issue could be minimized by placing the tube portion of the GDD far from the corneal endothelium and parallel to the iris plane. Because of the relatively large tube size, enough space is required into the anterior chamber for the tube. Consequently, pars plana or ciliary sulcus placement were developed as to minimize the risk of corneal endothelium cell damages⁵³.

Tube migration is another factor of corneal damages. The plate might migrate forward as a result of wound healing and consequently the tube may protrude further into the anterior chamber. Some micro-movement may occur over time, resulting in corneal endothelial touch. The other reason for this complication is shallow anterior chamber, appearing after an overfiltration or hypotony. Due to the reduction of space in the anterior chamber, the tube may touch the cornea and cause damages, such as corneal decompensation.

Table 1-2: Comparison of the most common Glaucoma Drainage Devices

	Baerveldt®	Molteno®	Ahmed®	Krupin®
Plate area [mm²]	250 or 350	135 or 270	184	194
Implant profile [mm]	0.84	1.65	1.9	2.54
Material	Smooth, pliable silicone with Barium	Rigid polypropylene	Rigid polypropylene or Silicone	Silicone
Tube external diameter [mm]	0.63	0.64	0.63	0.64
Tube internal diameter [mm]	0.3	0.34	0.3	0.38
Drainage tube	Non-valved	Non-valved	Valved	Valved
Manufacturer	Abbott Medical Optics	Molteno Ophthalmic Ltd.	New World Medical, Inc.	Eagle Vision, Inc.

1.7 Hypertensive phase

Several months after implanting a GDD, IOP often rises above 21 mmHg suggesting that the long-term control of the IOP is also a concern in glaucoma surgery management¹⁰. Even if the

causes are not well understood, there are different theories that were proposed suggesting that bleb fibrosis was responsible for late failure. The hypertensive phase is generally described as an IOP greater than 21 mmHg. The highest rate of incidence involving ocular hypertony has been related to the Ahmed implant (40-80%)^{19, 37, 38}. This postoperative elevated intraocular pressure is frequently caused by the formation of a capsular fibrosis around the implant¹⁰. The hypertensive phase is common to all glaucoma shunt designs and appears to depend on the materials and the shape or the size of the endplate^{54, 55}. Previous studies have demonstrated that silicone-made implants led to lower incidence of high postoperative IOP compared to the ones made of polypropylene^{55, 56}. In addition, the location where the plate of the GDD is positioned and the size of the plate may also influence the scarring response and fibrosis formation. The degree of IOP reduction and therefore the long-term success of any GDD depend on the capsular thickness and the surface area of encapsulation. A thinner capsule and a larger surface of encapsulation leads to increased diffusion of the aqueous humor, thereby to lower post-operative IOP. For instance, the smaller surface of the Ahmed as compared to the double-plate Molteno or Baerveldt may lead to lower diffusion of AH, therefore to higher IOP¹⁹. Nonetheless, there is an undetermined upper limit on the size of the endplate beyond which it may not improve outflow.

The AH contains some specific factors that enhance the fibrotic response, thereby influencing the filtration properties of the capsule and thus the level of hypertension⁵⁷. It has been hypothesized that the high AH flow rates evidenced with the Ahmed valve, carrying larger amounts of factors promoting fibrosis, would tend to increase the rate of fibrosis compared to non-valved implants with ligatures^{19, 5}. Hence, limiting the high AH flows in the early postoperative phase may have beneficiary effects for the long-term fibrotic response.

Comparison of Glaucoma Drainage Devices

There are numerous studies comparing the different glaucoma drainage devices currently available for the treatment of glaucoma. The average overall surgical success rate ranges between 72% and 79% among the five main drainage devices (Molteno single and double plate, Baerveldt, Ahmed, Krupin) with a statistically significant lower IOP after the operation^{5, 58}. These results demonstrate that GDDs have the potential to improve glaucoma filtering surgery outcome, however currently all GDDs exhibit complications due to poor flow control. New designs are needed to better control the flow and to improve the success of the procedure.

1.8 Requirements for next GDD generation

The ideal GDD would be the one that allows for the maintenance of IOP levels within the physiological range for the entire postoperative period. Because scarring tissue response, bleb formation and fibrosis are events influencing outflow resistance, one would ideally need a GDD with a variable resistance to compensate for the changes in outflow resistance occurring naturally and at different rates during the period following filtration surgery. The ideal situation for a glaucoma filtering surgery should be as follows: right after the insertion of the tube, its resistance to outflow should be maximal in order to keep the IOP high enough to prevent post-operative hypotony. Later on, the resistance should be reduced to maintain a proper control over the target IOP. Finally, the resistance of the GDD should be minimal, balancing the creation of fibrosis downstream.

Following the scenario envisioned above and given the fact that tissue scarring and bleb formation varies among different patients, the ideal glaucoma shunt should be of variable and adjustable resistance, adaptable for each patient. In fact, the picture of a faucet in the eye would be the best way to explain what is expected: this faucet would regulate the IOP by changing the resistance to aqueous humor outflow at any time and in a non-traumatic way.

In that prospect, the main body of work presented in this thesis shows the development and the testing of a new glaucoma drainage device. This implant is the first non-invasively adjustable glaucoma drainage device, which aims at providing a better solution to ophthalmologists by taking control of their patient's IOP and thus reducing the rate of related complications.

1.9 References

1. Congdon N, O'Colmain B, Klaver CC, et al. Causes and prevalence of visual impairment among adults in the United States. *Arch Ophthalmol* 2004;122:477-485.
2. Quigley HA, Broman AT. The number of people with glaucoma worldwide in 2010 and 2020. *Br J Ophthalmol* 2006;90:262-267.
3. Kwon YH, Fingert JH, Kuehn MH, Alward WL. Primary open-angle glaucoma. *N Engl J Med* 2009;360:1113-1124.
4. Bailey AK, Sarkisian SR, Jr. Complications of tube implants and their management. *Curr Opin Ophthalmol* 2014;25:148-153.
5. Hong CH, Arosemena A, Zurakowski D, Ayyala RS. Glaucoma drainage devices: a systematic literature review and current controversies. *Surv Ophthalmol* 2005;50:48-60.
6. Schnyder C. *Glaucoma*. Paris: Elsevier; 2005:463 p.
7. Bissig A, Feusier M, Mermoud A, Roy S. Deep sclerectomy with the Ex-PRESS X-200 implant for the surgical treatment of glaucoma. *Int Ophthalmol* 2010;30:661-668.
8. Desai MA, Gedde SJ, Feuer WJ, Shi W, Chen PP, Parrish RK, 2nd. Practice preferences for glaucoma surgery: a survey of the American Glaucoma Society in 2008. *Ophthalmic Surg Lasers Imaging* 2011;42:202-208.
9. Topouzis F, Coleman AL, Choplin N, et al. Follow-up of the original cohort with the Ahmed glaucoma valve implant. *Am J Ophthalmol* 1999;128:198-204.
10. Gedde SJ, Panarelli JF, Banitt MR, Lee RK. Evidenced-based comparison of aqueous shunts. *Curr Opin Ophthalmol* 2013;24:87-95.
11. Gedde SJ, Schiffman JC, Feuer WJ, Herndon LW, Brandt JD, Budenz DL. Three-year follow-up of the tube versus trabeculectomy study. *Am J Ophthalmol* 2009;148:670-684.
12. Cairns JE. Trabeculectomy. Preliminary report of a new method. *Am J Ophthalmol* 1968;66:673-679.
13. Beckers HJ, Kinders KC, Webers CA. Five-year results of trabeculectomy with mitomycin C. *Graefes Arch Clin Exp Ophthalmol* 2003;241:106-110.
14. Bhatia J. Outcome of trabeculectomy surgery in primary open angle glaucoma. *Oman Med J* 2008;23:86-89.
15. Costa VP, Arcieri ES. Hypotony maculopathy. *Acta Ophthalmol Scand* 2007;85:586-597.
16. Fyodorov SN, Kozlov V. I. et al. Nonpenetrating deep sclerectomy in open angle glaucoma. *Ophthalmic Surg* 1990;3:52-55.
17. Kozlov VI, Bagrov, S. N., Anisimova, S. Y., et al. Nonpenetrating deep sclerectomy with collagen. *Eye Microsurgery* 1990;3:44-46.
18. Molteno AC. New implant for drainage in glaucoma. Clinical trial. *Br J Ophthalmol* 1969;53:606-615.
19. Ayyala RS, Zurakowski D, Monshizadeh R, et al. Comparison of double-plate Molteno and Ahmed glaucoma valve in patients with advanced uncontrolled glaucoma. *Ophthalmic Surg Lasers* 2002;33:94-101.
20. Heuer DK, Lloyd MA, Abrams DA, et al. Which is better? One or two? A randomized clinical trial of single-plate versus double-plate Molteno implantation for glaucomas in aphakia and pseudophakia. *Ophthalmology* 1992;99:1512-1519.
21. Britt MT, LaBree LD, Lloyd MA, et al. Randomized clinical trial of the 350-mm² versus the 500-mm² Baerveldt implant: longer term results: is bigger better? *Ophthalmology* 1999;106:2312-2318.
22. Ceballos EM, Parrish RK, 2nd. Plain film imaging of Baerveldt glaucoma drainage implants. *AJNR Am J Neuroradiol* 2002;23:935-937.
23. Krupin T, Podos SM, Becker B, Newkirk JB. Valve implants in filtering surgery. *Am J Ophthalmol* 1976;81:232-235.

24. Ayyala RS, Zurakowski D, Smith JA, et al. A clinical study of the Ahmed glaucoma valve implant in advanced glaucoma. *Ophthalmology* 1998;105:1968-1976.
25. Ramulu PY, Corcoran KJ, Corcoran SL, Robin AL. Utilization of various glaucoma surgeries and procedures in Medicare beneficiaries from 1995 to 2004. *Ophthalmology* 2007;114:2265-2270.
26. Dahan E, Carmichael TR. Implantation of a miniature glaucoma device under a scleral flap. *J Glaucoma* 2005;14:98-102.
27. De Feo F, Bagnis A, Bricola G, Scotto R, Traverso CE. Efficacy and safety of a steel drainage device implanted under a scleral flap. *Can J Ophthalmol* 2009;44:457-462.
28. Kanner EM, Netland PA, Sarkisian SR, Jr., Du H. Ex-PRESS miniature glaucoma device implanted under a scleral flap alone or combined with phacoemulsification cataract surgery. *J Glaucoma* 2009;18:488-491.
29. Rivier D, Roy S, Mermoud A. Ex-PRESS R-50 miniature glaucoma implant insertion under the conjunctiva combined with cataract extraction. *J Cataract Refract Surg* 2007;33:1946-1952.
30. Gedde SJ. Results from the tube versus trabeculectomy study. *Middle East Afr J Ophthalmol* 2009;16:107-111.
31. Gedde SJ, Herndon LW, Brandt JD, Budenz DL, Feuer WJ, Schiffman JC. Postoperative complications in the Tube Versus Trabeculectomy (TVT) study during five years of follow-up. *Am J Ophthalmol* 2012;153:804-814 e801.
32. Gedde SJ, Schiffman JC, Feuer WJ, Herndon LW, Brandt JD, Budenz DL. Treatment outcomes in the Tube Versus Trabeculectomy (TVT) study after five years of follow-up. *Am J Ophthalmol* 2012;153:789-803 e782.
33. Traverso CE, De Feo F, Messas-Kaplan A, et al. Long term effect on IOP of a stainless steel glaucoma drainage implant (Ex-PRESS) in combined surgery with phacoemulsification. *Br J Ophthalmol* 2005;89:425-429.
34. Wilson MR, Mendis U, Smith SD, Paliwal A. Ahmed glaucoma valve implant vs trabeculectomy in the surgical treatment of glaucoma: a randomized clinical trial. *Am J Ophthalmol* 2000;130:267-273.
35. Stein JD, McCoy AN, Asrani S, et al. Surgical management of hypotony owing to overfiltration in eyes receiving glaucoma drainage devices. *J Glaucoma* 2009;18:638-641.
36. Syed HM, Law SK, Nam SH, Li G, Caprioli J, Coleman A. Baerveldt-350 implant versus Ahmed valve for refractory glaucoma: a case-controlled comparison. *J Glaucoma* 2004;13:38-45.
37. Wilson MR, Mendis U, Paliwal A, Haynatzka V. Long-term follow-up of primary glaucoma surgery with Ahmed glaucoma valve implant versus trabeculectomy. *Am J Ophthalmol* 2003;136:464-470.
38. Nouri-Mahdavi K, Caprioli J. Evaluation of the hypertensive phase after insertion of the Ahmed Glaucoma Valve. *Am J Ophthalmol* 2003;136:1001-1008.
39. Coleman AL, Wilson MR, Tam M, et al. Initial clinical experience with the Ahmed glaucoma valve implant--correction. *Am J Ophthalmol* 1995;120:684.
40. Feldman RM, el-Harazi SM, Villanueva G. Valve membrane adhesion as a cause of Ahmed glaucoma valve failure. *J Glaucoma* 1997;6:10-12.
41. Freedman J. Management of the Molteno silicone tube in corneal transplant surgery. *Ophthalmic Surg Lasers* 1998;29:432-434.
42. Sarkisian SR, Jr. Tube shunt complications and their prevention. *Curr Opin Ophthalmol* 2009;20:126-130.
43. Smith SL, Starita RJ, Fellman RL, Lynn JR. Early clinical experience with the Baerveldt 350-mm² glaucoma implant and associated extraocular muscle imbalance. *Ophthalmology* 1993;100:914-918.
44. Munoz M, Parrish RK, 2nd. Strabismus following implantation of Baerveldt drainage devices. *Arch Ophthalmol* 1993;111:1096-1099.

45. Lama PJ, Fechtner RD. Tube erosion following insertion of a glaucoma drainage device with a pericardial patch graft. *Arch Ophthalmol* 1999;117:1243-1244.
46. King AJ, Azuara-Blanco A. Pericardial patch melting following glaucoma implant insertion. *Eye (Lond)* 2001;15:236-237.
47. Maris PJ, Jr., Ishida K, Netland PA. Comparison of trabeculectomy with Ex-PRESS miniature glaucoma device implanted under scleral flap. *J Glaucoma* 2007;16:14-19.
48. Huang MC, Netland PA, Coleman AL, Siegner SW, Moster MR, Hill RA. Intermediate-term clinical experience with the Ahmed Glaucoma Valve implant. *Am J Ophthalmol* 1999;127:27-33.
49. Fellenbaum PS, Almeida AR, Minckler DS, Sidoti PA, Baerveldt G, Heuer DK. Krupin disk implantation for complicated glaucomas. *Ophthalmology* 1994;101:1178-1182.
50. Patel S, Pasquale LR. Glaucoma drainage devices: a review of the past, present, and future. *Semin Ophthalmol* 2010;25:265-270.
51. Egbert PR, Lieberman MF. Internal suture occlusion of the Molteno glaucoma implant for the prevention of postoperative hypotony. *Ophthalmic Surg* 1989;20:53-56.
52. Stewart W, Feldman RM, Gross RL. Collagen plug occlusion of Molteno tube shunts. *Ophthalmic Surg* 1993;24:47-48.
53. Weiner A, Cohn AD, Balasubramaniam M, Weiner AJ. Glaucoma tube shunt implantation through the ciliary sulcus in pseudophakic eyes with high risk of corneal decompensation. *J Glaucoma* 2010;19:405-411.
54. Ayyala RS, Michelini-Norris B, Flores A, Haller E, Margo CE. Comparison of different biomaterials for glaucoma drainage devices: part 2. *Arch Ophthalmol* 2000;118:1081-1084.
55. Hinkle DM, Zurakowski D, Ayyala RS. A comparison of the polypropylene plate Ahmed glaucoma valve to the silicone plate Ahmed glaucoma flexible valve. *Eur J Ophthalmol* 2007;17:696-701.
56. Ishida K, Netland PA, Costa VP, Shiroma L, Khan B, Ahmed, II. Comparison of polypropylene and silicone Ahmed Glaucoma Valves. *Ophthalmology* 2006;113:1320-1326.
57. el-Sayyad F, el-Maghraby A, Helal M, Amayem A. The use of releasable sutures in Molteno glaucoma implant procedures to reduce postoperative hypotony. *Ophthalmic Surg* 1991;22:82-84.
58. Schwartz KS, Lee RK, Gedde SJ. Glaucoma drainage implants: a critical comparison of types. *Curr Opin Ophthalmol* 2006;17:181-189.

Chapters

The main body of the thesis contains 4 chapters, each chapter being a separate paper either already published (3) or submitted for publication (1) in important refereed journals in the fields of ophthalmology or bioengineering.

Paper 1

Glaucoma is often associated with an increase of the intraocular pressure (IOP), which results from an increase in the outflow resistance to aqueous humor outflow. Several treatments are proposed to reduce and stabilize the IOP, including medications, filtering surgery and glaucoma drainage devices (GDD). So far computational fluid dynamics (CFD) modeling of the eye drainage system has not yet been well studied. Therefore our goal was to provide a 3D CFD model of the eye based on the anatomy of a real human eye. Such a tool would serve for future evaluation of new glaucoma surgical techniques involving, for example, GDD. The model was based on stacks of microphotographs from human eye slides from which digital processing of the images of the eye structure and 3D reconstruction of the model were performed. Simulations of the distribution of pressure and flow velocity in the model of a healthy eye gave results comparable to physiology references. Mimicking glaucoma conditions led to an increase in the level of IOP and simulated IOP decreased significantly to lower values after a filtering procedure. Further refinements in the boundary conditions for the filtering procedure shall improve the accuracy of this innovative tool for modeling glaucoma surgery.

Paper 2

Previous mathematical models and CFD simulations allowed the optimization and development of an Adjustable Glaucoma Drainage Device. This 2nd paper is focused on the testing of a new experimental noninvasively adjustable glaucoma drainage device (AGDD) that allows for the control of its outflow resistance to modulate intraocular pressure (IOP) in a

customized fashion.

Six AGDDs were directly connected to a pressure transducer and a perfusion system was continuously delivering a saline solution at rate of 2 $\mu\text{L}/\text{min}$. The steady-state pressure was measured and reported as a function of the angular position of the AGDD disk. Ex vivo experiments were conducted on six freshly enucleated rabbit eyes. The IOP was measured, and the flow rate was increased with a syringe pump to simulate elevated IOP associated with glaucoma. After insertion of the implant in the anterior chamber, the position of the disk was sequentially adjusted.

The relation between the pressure drop and the angular position of the AGDD disk is nonlinear. The functional range lies between 80° and 130° , which allows for four or five different reproducible adjustment positions. Above 130° the implant is considered to be closed (no outflow), and below 80° it is considered to be open (minimum resistance to flow).

The resistance to outflow of the experimental AGDD can be adjusted to keep IOP in the desired physiological range. This feature could be useful for addressing the risk of hypotony in the early postoperative stages and could provide a means to achieve optimal IOP under a wide range of postoperative conditions.

Paper 3

This work reports on the *in vivo* testing of a novel non-invasively adjustable glaucoma drainage device (AGDD), which features an adjustable outflow resistance and to assess the safety and efficiency of this implant.

Under general anesthesia, the AGDD was implanted under a scleral flap on 7 white New-Zealand rabbits for a duration of 4 months, in a way analogous to the Ex-PRESS® device. The device was set in an operationally closed position. The IOP was measured on a regular basis on both the operated and the control eyes using a rebound tonometer. Once a month the AGDD was adjusted non-invasively from its fully closed position to its fully open position and the resulting pressure drop was measured. The contralateral eye was not operated and served as control. After sacrifice the eyes were collected for histology evaluation.

The mean preoperative IOP was 11.1 ± 2.4 mmHg. The IOP was significantly lower for the operated eye (6.8 ± 2 mmHg) compared to the non-operated eye (13.1 ± 1.6 mmHg) during the first eight days after surgery. When opening the AGDD from its fully closed to fully open

position, the IOP dropped significantly from 11.2 ± 2.9 mmHg down to 4.8 ± 0.9 mmHg ($p < 0.05$).

Implanting the AGDD is a safe and uncomplicated surgical procedure. The fluidic resistance was non-invasively adjustable during the entire post-operative period with the AGDD between its fully closed and fully open positions.

Paper 4

Paper 4 is neither related to the glaucoma drainage devices field nor to glaucoma itself. It represents a side project developed at the beginning of the thesis focusing on methods to evaluate or estimate the compliance of the eye vessels, a quantity of interest because of its potential implication in various retinal diseases. In specific, the goal of the study was to develop and validate a methodology to measure the compliance of the vascular network in the eye using biomechanical parameters, namely arterial pressure, intraocular pressure (IOP), and ocular compliance of the eyeball (OC).

In vitro experiments were conducted on 6 freshly enucleated rabbit eyes. An inflatable catheter was inserted in the posterior chamber. The balloon was inflated and its volume changed periodically at a rate of 1–2 Hz, yielding variations in the intraocular volume; thus, emulating the volume pulsations of the vascular network in the eye. The IOP was measured continuously with a pressure transducer and the OC was calculated using the outflow facility. The compliance of the balloon, mimicking the compliance of the vascular network, was estimated indirectly from the measurements of IOP, balloon pressure, and OC. The estimated balloon compliance was compared to direct estimates of balloon compliance, based on the balloon pressure-volume curve. The in vivo part of the study included 5 white New-Zealand rabbits. The method to estimate the vascular compliance of the eye was tested under normal conditions and after administration of norepinephrine, which induced a vasoconstriction leading to reduction in vascular compliance.

In vitro comparison of direct versus indirect estimates of compliance showed a difference that was not significant (0.075 vs. 0.077 $\mu\text{L}/\text{mmHg}$, $P = 0.86$). Results from the in vivo study indicated that norepinephrine significantly increased the arterial pulse pressure amplitude, while compliance of vascular network of the eye decreased from 0.18 ± 0.12 to 0.10 ± 0.08 $\mu\text{L}/\text{mm Hg}$ ($P = 0.001$).

We concluded that the eye vascular compliance can be accurately predicted using the IOP, arterial pressure, and OC of the eyeball.

Chapter 2 : 1st Paper

Published in Medical Engineering and Physics, December 2012.

3D Simulation of the Aqueous Flow in the Human Eye

Adan Villamarin, MSc¹; Sylvain Roy, MD, PhD^{1,2}; Reda Hasballa, MSc¹; Orestis Vardoulis,
MSc¹; Philippe Reymond, PhD¹; Nikos Stergiopoulos, PhD¹.

¹Swiss Federal Institute of Technology, Laboratory of Hemodynamics and Cardiovascular
Technology, Lausanne, Switzerland; ²Glaucoma Center, Montchoisi Clinic Lausanne,
Switzerland.

Medical Engineering & Physics 34 (2012) 1462–1470

Doi: 10.1016/j.medengphy.2012.02.007

Submitted: August 16, 2011

Accepted: February 7, 2012

2.1 Introduction

Glaucoma is one of the leading causes of blindness in the world [1]. It generally results from a decrease of the aqueous humor (AH) outflow, which leads to an increase in the intraocular pressure (IOP) [2]. As a consequence the retina ganglion cells progressively suffer irreversible damages that lead to visual field reduction and eventually to blindness [3]. Many therapeutic options are available to reduce and control IOP to prevent glaucoma damages. Such therapeutic tools include the anti-glaucoma medications, the filtering surgery to remove the obstacle to egress of AH, which may include glaucoma drainage device (GDD) implantation, or the selective destruction of the ciliary body, to name a few [4], [5].

Aqueous humor is produced in the posterior chamber at the level of the ciliary body at a rate of 2-3 $\mu\text{l}/\text{min}$ [6]. The fluid then flows through the posterior portion of the iris and the anterior surface of the lens through the pupil to enter the anterior chamber. At this point two outflow pathways exist: the first one is the conventional pathway where the aqueous humor flows through the trabecular meshwork (TM), which is a latticed structure composed of three layers, the uveal meshwork, the corneoscleral meshwork, and the juxtacanalicular or cribriform meshwork. Cells embedded in a dense extracellular matrix form the latter and most of the resistance to the flow egress is commonly believed to lie at that level [7]. The second one is called the uveoscleral pathway and refers to the aqueous humor leaving the anterior chamber by diffusion through intercellular spaces among ciliary muscle fibers [8]. This pathway represents about 10% of the total aqueous humor outflow [9].

After passing through these layers, aqueous humour enters the Schlemm's canal (SC). This channel, which is located at the transitional zone between the cornea and the sclera, is linked to the veins at the surface of the sclera via 25-30 collecting channels (CC). The SC (oval shaped) has a mean diameter of about 120 μm [10] and a total circumference around 35 mm.

Finally AH is drained out of the eye through episcleral veins to get mixed with the bloodstream [11].

The fluid dynamics of AH in the anterior chamber and the role of the trabecular meshwork (TM) and CC are not fully understood. Consequently, computational simulation of AH flow in the anterior chamber can provide enlightening information about ocular diseases such as glaucoma where the outflow of AH is obstructed.

Several models have previously reported temperature distribution and flow mechanisms in the anterior chamber of the eye using simulations and mathematical models [12-17]. However, the assumptions and simplifications made in these models may limit their accuracy. Furthermore, none of these models included the TM to obtain flow field inside the anterior chamber nor did they analyse its effects on IOP. Kumar et al. [18] were the first to report a flow simulation where the geometry of the TM was directly modelled. Intraocular pressure results were close to experimental observations and they concluded that buoyancy was the driving mechanism for the AH flow and TM accounted for the most resistive spot. Nevertheless this model was based on rabbit eyes and specific geometrical considerations have been made compared to a human eye.

Based on these observations an exact model of the human eye including TM, SC and CC structures is welcomed to better understand the outflow drainage system and to evaluate the velocity streamlines and pressure contours in healthy eyes as well as in eyes undergoing filtering surgery.

Thus the goal of this study was to develop a 3D model of the human eye based on a post-mortem human eye and to establish the aqueous humor flow characteristics under physiological and pathological conditions such as primary open-angle glaucoma. This tool would serve as a base for further simulations and evaluations of different glaucoma surgeries such as trabeculectomy [19] or implantation of GDDs.

2.2 Material and Methods

2.2.1 Histology preparation

An enucleated human eye from eye banking (Cleveland Eye Bank, OH, USA) and not suitable for corneal grafting, was perfused at around 15 mmHg and fixed in a 4% formaldehyde solution for two hours. The globe was gradually dehydrated and embedded in wax. It was then cut at a thickness of 6 μm , each section being 200 μm apart from the other. Slides were stained with Masson's trichrome.

2.2.2 Image Reconstruction

Each slide was photographed using a digital camera mounted on a microscope at a 4x magnification. The entire stack of images from the histological slices was used to reconstruct the eye structures. Great attention was given to details in the geometry of the structures such as the trabeculum meshwork, the Schlemm's canal and the collector channels. The contours of the anatomical structures were extracted manually.

2.2.3 3D geometry

The different structures obtained from the stack of histology images were imported in Rhinoceros software (Robert McNeel & Associates, WA, USA) for processing. Every geometrical object corresponding to a particular eye structure (cornea, lens, iris, TM, SC, CC and the ciliary body) was treated separately to remove defaults generated during image extraction such as non-manifold edges, duplicate elements and degenerated faces.

Missing structures such as the hyaloid membrane and the collector channels ($n = 26$) were added to the model. A volumetric mesh was created with ICEM CFD software (ANSYS Inc., Canonsburg, PA, USA) and exported to ANSYS CFX (ANSYS Inc., Canonsburg, PA, USA) for the fluid simulation. Evolution of the 3D construction is depicted in figure 2-1.

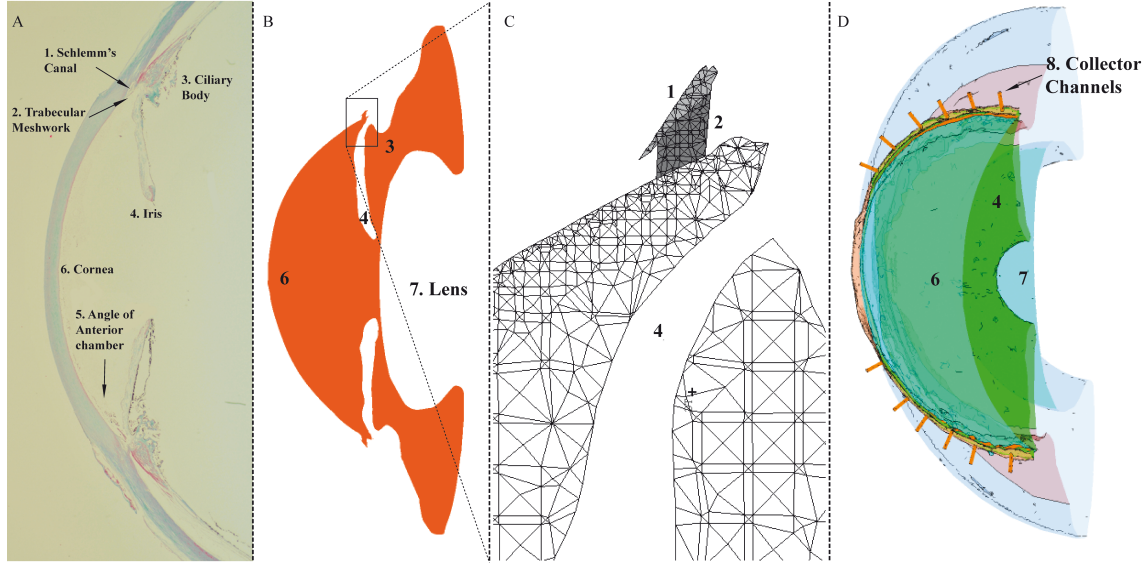


Figure 2-1: Evolution of the 3D human eye model reconstruction. (A) Histological slice. (B) 2D model extracted from histology. (C) Details of the TM and the SC with the used mesh. (D) 3D mesh of the human eye model.

2.2.4 Governing equation

In the present study the motion of AH is considered in the anterior and posterior chamber. Navier-Stokes equations for incompressible fluid flow were used to model the motion of AH in x , y and z directions.

$$\rho(\mathbf{v} \cdot \nabla \mathbf{v}) = -\nabla p + \mu \nabla^2 \mathbf{v} + \rho \mathbf{g} \quad (1)$$

where \mathbf{v} is the velocity; p is the pressure; ρ is the density of the fluid; and μ is the dynamic viscosity; whereas \mathbf{g} represents the gravitational acceleration.

The Boussinesq approximation was used to represent the effect of buoyancy due to the temperature gradient. This approximation states that the density of liquid changes with temperature and negligibly with pressure. Boussinesq approximation can be given by:

$$\rho = \rho_0 \left[1 - \beta (T - T_{ref}) \right] \quad (2)$$

where ρ_0 defines the reference density; β is the volume expansion coefficient; and T_{ref} is the reference temperature. Thus by combining the compact Navier-Stokes equation and

Boussinesq approximation (2), the resulting equation is the Navier-Stokes equation with an additional term for thermal change in fluid density given by equation (3).

$$\rho \mathbf{v} \cdot \nabla \mathbf{v} = -\nabla p + \mu \nabla^2 \mathbf{v} + \rho_0 \mathbf{g} \beta (T - T_{ref}) \quad (3)$$

Equation (4) describes the continuity that AH for steady and incompressible flow has to satisfy in the anterior chamber.

$$\nabla \cdot \mathbf{v} = 0 \quad (4)$$

Finally, equation (5) describes the convective and diffusive transport of energy by AH where viscous dissipation effect has been neglected.

$$\rho C_p \mathbf{v} \cdot \nabla T = k \nabla^2 T \quad (5)$$

where k is the thermal conductivity and C_p is the heat capacity. Values are summarized in Table 2-1.

Table 2-1: Properties of AH used in the model

Properties	Value	Source
AH density, ρ	1000 kg·m ⁻³	Water Properties
AH viscosity, μ	0.001 kg·m ⁻¹ ·s ⁻¹	Kumar et al. ¹⁸
AH thermal conductivity, K	0.6 W·m ⁻¹ ·K ⁻¹	Kumar et al. ¹⁸
AH specific heat, C_p	4182 J·kg ⁻¹ ·K ⁻¹	Water Properties
Volume expansion coefficient, β	0.0003 K ⁻¹	Water Properties
Cornea anterior surface temperature, T_a	35 °C	Kumar et al. ¹⁸
Thermal conductivity of cornea, K	0.58 W·m ⁻¹ ·K ⁻¹	Heys et al. ¹⁴

2.2.5 Permeability

The permeability characterizes the ability of a porous material to diffuse fluids. This parameter is used to define the resistance of the outflow through the TM. Darcy's law defines permeability of TM [20]:

$$\alpha = \frac{\mu}{\Delta P} \Delta e v \quad (4)$$

where α being the permeability, ΔP is the pressure change, μ is the viscosity, Δe is the thickness of the porous domain, and v is the velocity component.

2.2.6 Boundary conditions

The iris, lens and cornea are modeled as stationary rigid boundaries, and no-slip boundary condition is imposed along these surfaces. The temperature of the iris and the lens is assumed to be at 37°C. The temperature at the surface of the cornea is generally considered to lie between 33 and 35 °C [21], and was assumed in this study to be 35°C. The temperature drop between the iris and the cornea provides the buoyant force mechanism to drive AH in the anterior chamber.

The ciliary body was defined as the inflow region to simulate AH production at a rate of 3 μ l/min. The static pressure imposed at the collecting channels was estimated at 7 mmHg defining the pressure inside the episcleral veins. The trabecular meshwork was modeled as a porous domain with the corresponding permeability parameter fitted to obtain a suitable pressure change between the anterior chamber and the CC. Aqueous humor secreted by the ciliary body as well as the TM was assumed to be at 37°C.

The working IOP condition to mimic the healthy model used in the different simulations was defined by an IOP of 13.5 mmHg while the glaucomatous case was defined with an IOP of 27 mmHg.

2.2.7 Glaucoma Surgery

A scleral flap measuring $5 \times 5 \text{ mm}^2$ and $300 \text{ }\mu\text{m}$ thick was created in the model representing glaucoma surgery cases. Nine CC were added to the scleral flap where the static pressure is equal to the pressure of the episcleral veins as described previously.

Trabeculectomy is a standard procedure for open-angle glaucoma patients initially described by Cairns [19] in the late 60's. Briefly, in our simulation, it was modeled as a hole of $400 \text{ }\mu\text{m}$ in diameter located in the irido-corneal angle in the anterior chamber, passing through the SC and the TM, running parallel to the horizontal plane of the iris. This hole creates a direct link between the anterior chamber of the eye and the inner space of the scleral flap to increase the AH outflow.

The glaucoma drainage implant used in this model was the Ex-PRESS™ V50® (Ex-PRESS, Alcon Inc., Hünenberg, CH). A computer assisted design (CAD) model of the device was inserted in the 3D eye through the SC and the TM of the anterior chamber angle, parallel to the plane of the iris.

2.3 Results

The mesh of the anterior and posterior chamber as modeled contains 5,284,065 tetrahedral elements.

The Schlemm's canal is variable in appearance and in size and is represented by a single channel with a mean diameter of $140 \text{ }\mu\text{m}$ ($\pm 40 \text{ }\mu\text{m}$).

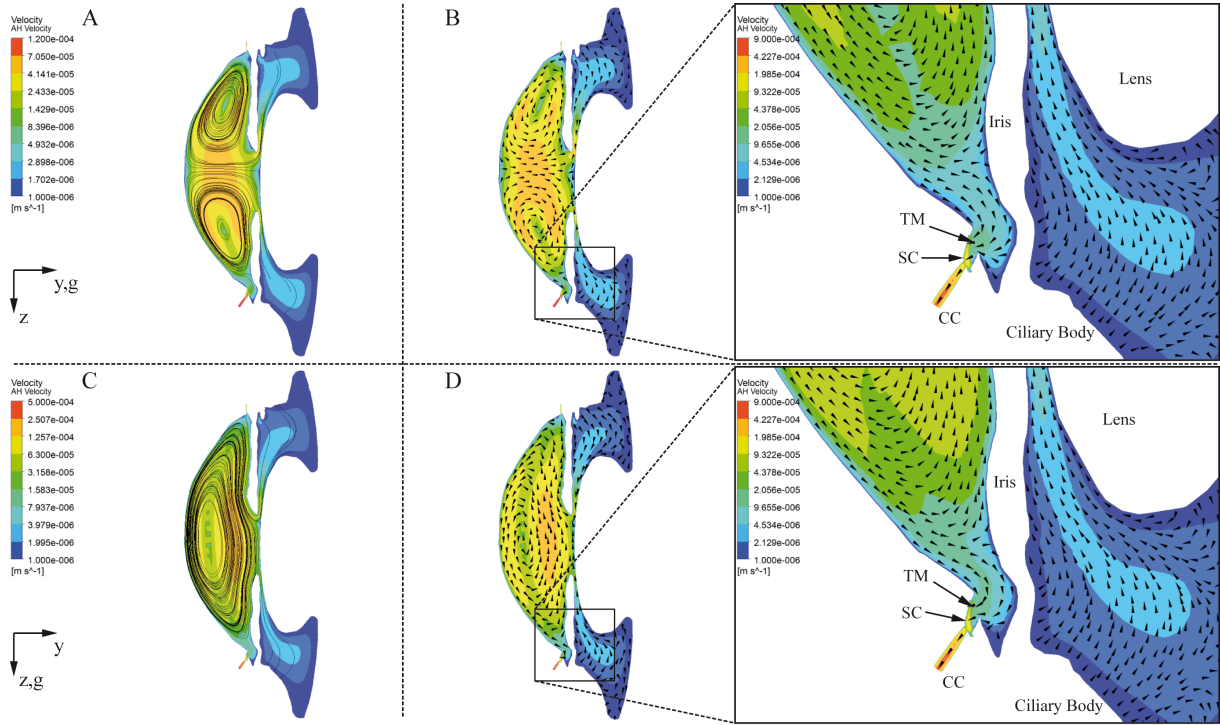


Figure 2-2: Contour of velocity magnitude and velocity vectors in anterior chamber with gravity in y (A streamlines, B vectors) and z (C streamlines, D vectors) directions, respectively. $\Delta T = 2^\circ\text{C}$.

2.3.1 Aqueous Humor Velocity

Figures 2-2A and 2-2B show the velocity distribution with the gravity in the y direction, perpendicular to the iris plane. This would correspond to the orientation of the eye for a patient in supine position. The AH is secreted by the ciliary body and then flows through the iris-lens gap where the velocity increases up to $7 \cdot 10^{-2} \text{ mm s}^{-1}$. After reaching the anterior chamber through the pupil, AH climbs towards the cornea where the velocity of the streamlines increases in the mid-portion up to $6 \cdot 10^{-2} \text{ mm s}^{-1}$. The streamlines then descend along the cornea curvature down to the irido-corneal angle where they could either exit through the TM or proceed further along the iris surface and then get mixed with the fluid flow entering the chamber, creating a recirculation zone. The highest velocity values (0.9 mm s^{-1}) are present in the SC and through the CC.

Figures 2-2C and 2-2D show the velocity distribution when gravity is applied in the z direction, parallel to the iris plane. This would be the case for a patient in a sitting position. In this model the warmer AH rises upward along the iris plane toward the apex of the irido-corneal angle. There AH could leave through the TM or go along the posterior surface of the cornea down to the lower portion of the irido-corneal angle. Again there AH can leave via TM or climb along the iris surface. It gets re-mixed with AH coming from the posterior

chamber upon reaching the pupil area. A recirculation zone is created in the whole anterior chamber portion. Aqueous humor finally exits through the pores of the TM joining the SC and CC. High velocities data are present in the SC and the CC (0.9 mm s^{-1}) and near the central portion of the iris surface (0.2 mm s^{-1}).

Velocities in the anterior chamber between healthy and glaucomatous simulations are similar.

2.3.2 Permeability

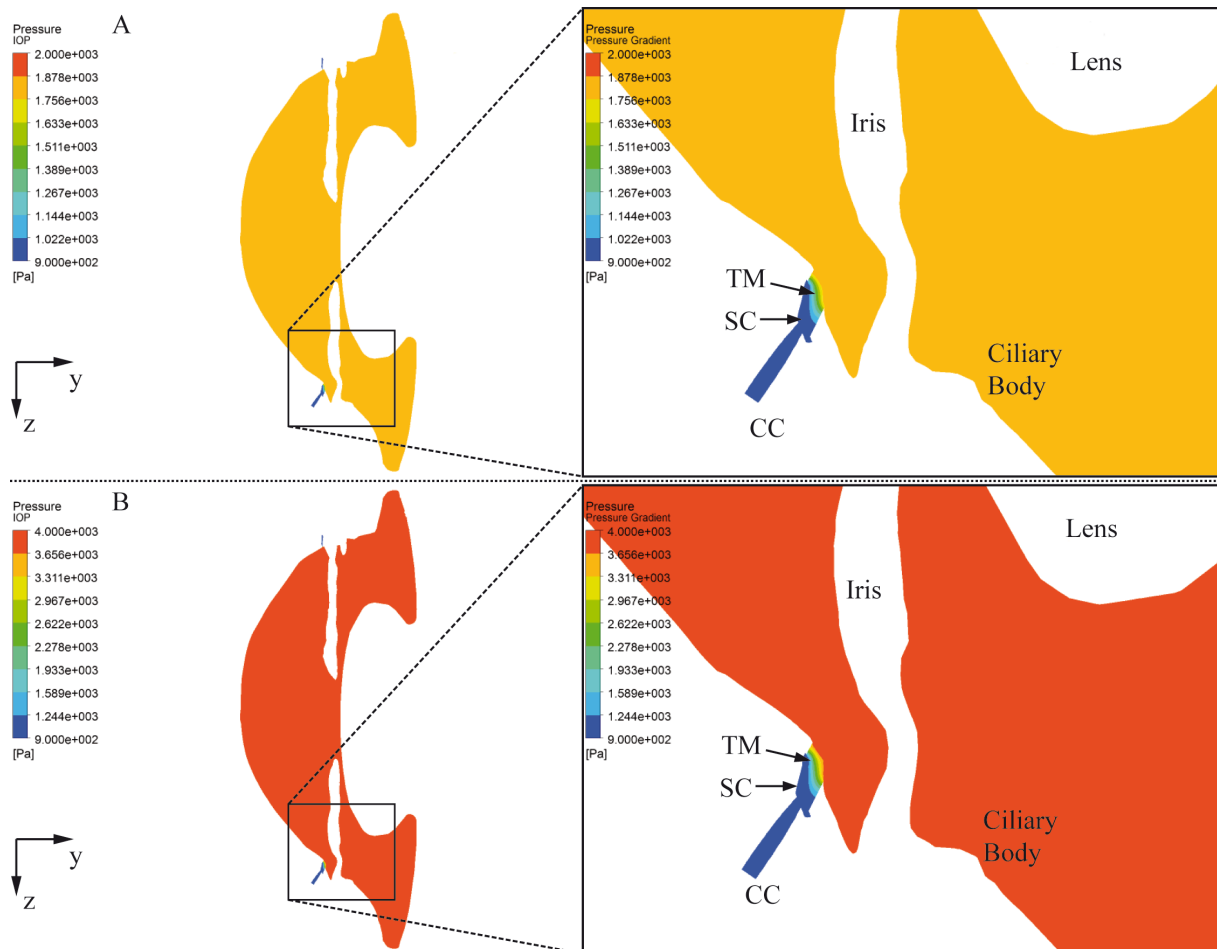


Figure 2-3: Contour of pressure in a healthy (A) and a glaucomatous (B) eye model with respective details of the trabecular meshwork and Schlemm's canal.

Aqueous flow modeling showed the pressure distribution in healthy and glaucoma simulation in the posterior and the anterior chambers, the trabecular meshwork, the SC and the CC (Figure 2-3A and 2-3B). The resistance of the TM to AH outflow determines the pressure drop between the anterior chamber and the episcleral veins. Several values of TM permeability were tested to define the IOP (Figure 2-4). Experimentations demonstrate that

the pressure drop in the anterior chamber is exponentially correlated to the permeability of the TM.

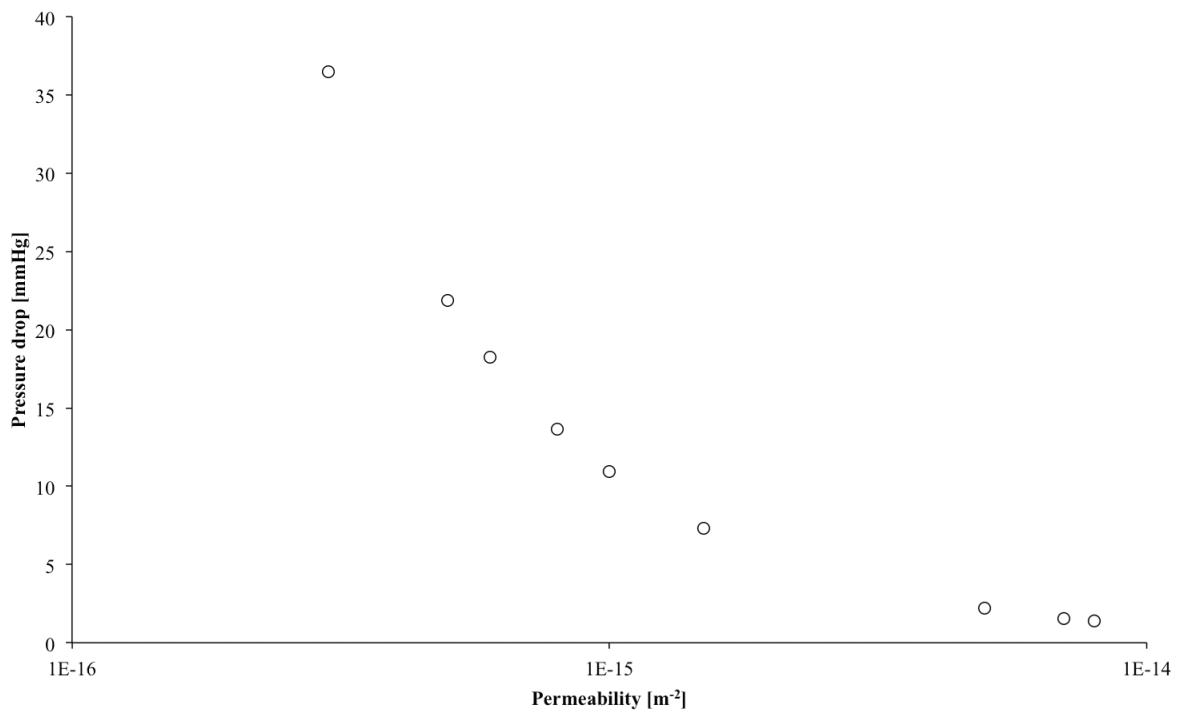


Figure 2-4: Graph representing the pressure drop (IOP – CC pressure) in function of the trabecular meshwork permeability (log – log plot). In this model the TM was set to $1.5 \cdot 10^{-15} m^2$ and $5 \cdot 10^{-16} m^2$ for normal and glaucoma simulations, respectively, in order to achieve an IOP of 13.5 mmHg for normal and 27 mmHg for glaucoma. Aqueous humor pressure remains constant in the anterior chamber from the ciliary body to the TM, while a pressure gradient through the TM is generated down to the episcleral vein's pressure.

2.3.3 Wall shear stress

Wall shear stress (WSS) in SC and through CC is represented in figure 2-5A & 2-5B. Magnitude of WSS was found to be higher at the proximal opening of the CC with a value of 0.012 Pa. In this case, WSS in SC and CC is not influenced by the orientation of the eye.

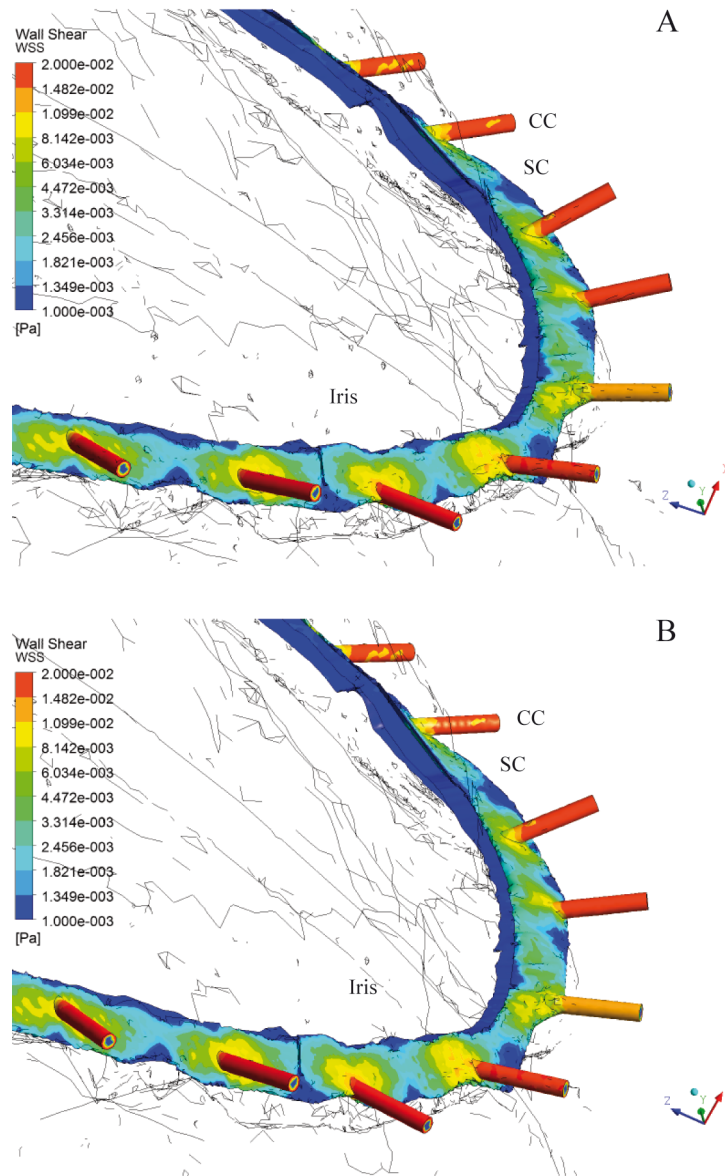


Figure 2-5: Wall shear stress in Schlemm's canal and collector channels for gravity in y direction (A) and z direction (B).

On the other hand, the shear stress contours of the iris (figure 2-6) and the corneal surfaces (figure 2-7) demonstrate a difference between the vertical and the horizontal position of the eye. Clearly both surfaces are subjected to higher shear stresses in the vertical orientation. In this orientation wall shear stress is maximal in the inner periphery of the iris, whereas the peak is reached on the mid-periphery of the cornea in the horizontal position. Shear stresses in the vertical orientation show maximal values on half of the iris and on the cornea along a horizontal band. For instance, on the corneal surface in respect with the vertical orientation of the eye, WSS is equal to $6.5 \cdot 10^{-4}$ Pa further maximal value while WSS is $2.8 \cdot 10^{-4}$ Pa on the horizontal reference plane.

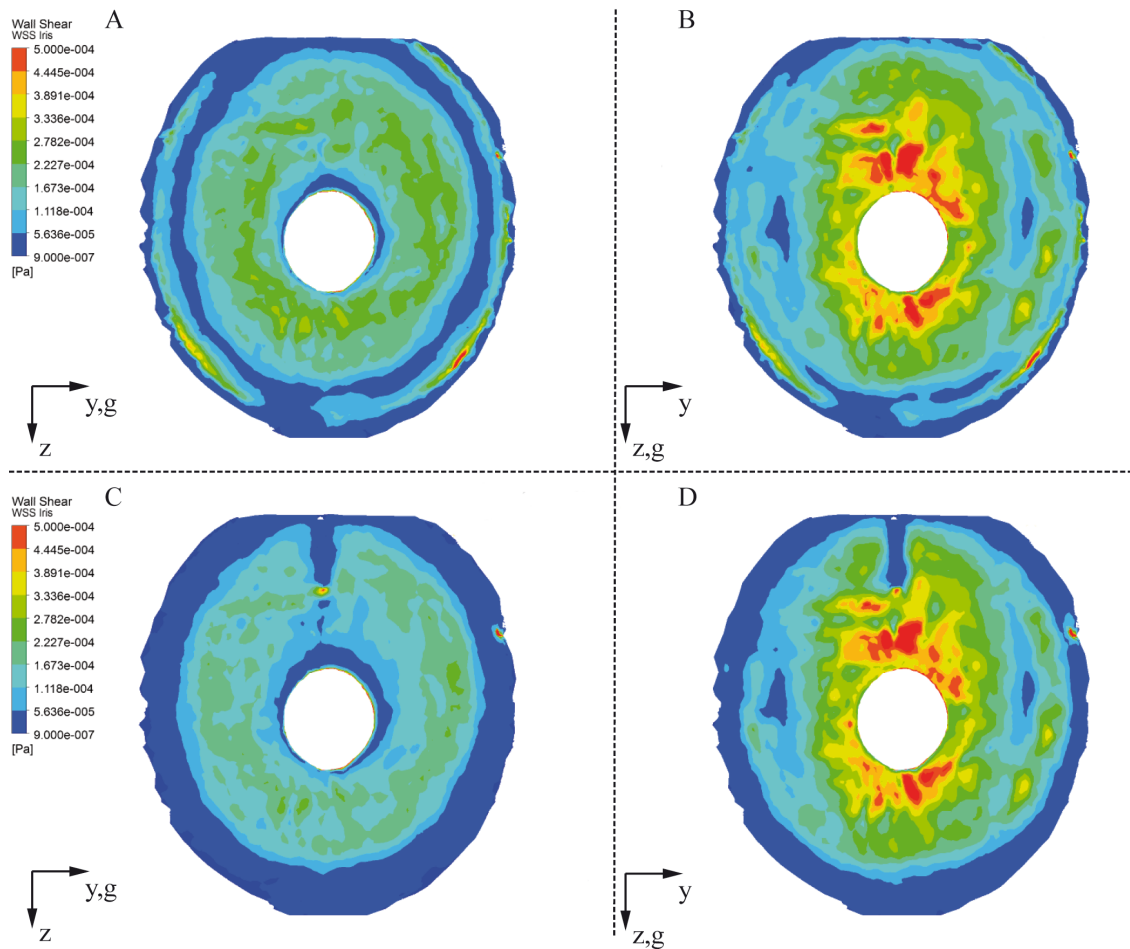


Figure 2-6: Shear stress in iris surface with gravity in y direction (A), z direction (B), and in presence of Ex-PRESS V50™ for y direction (C) and z direction (D).

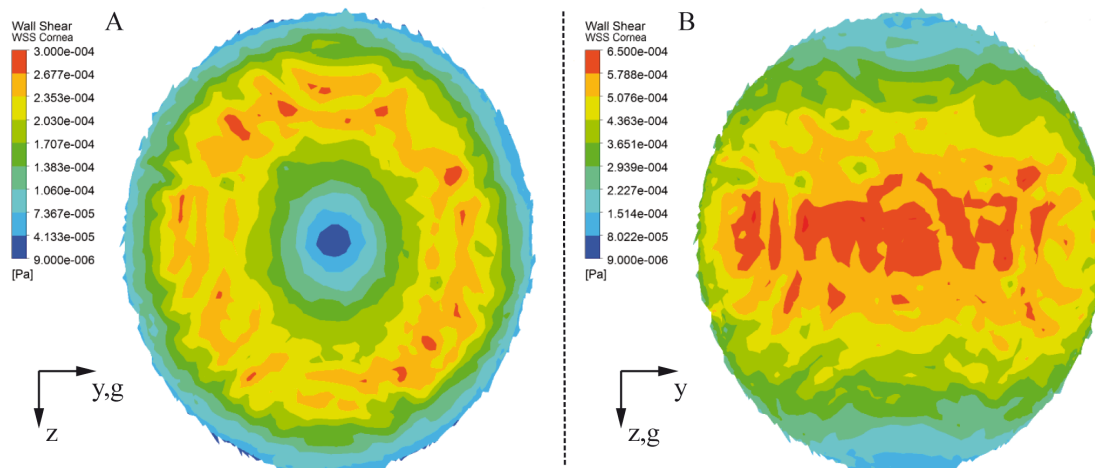


Figure 2-7: Shear stress in corneal surface with gravity in y direction (A) and z direction (B).

2.3.4 Effect of glaucoma surgery

The velocity contours of the flow passing through the device and the hole made by the trabeculectomy are depicted (figure 2-8 & 2-9). Velocities are higher for the model involving

the drainage device ($5 \cdot 10^{-3} \text{ m s}^{-1}$) due to its smaller diameter and to the presence of a resistor shaft. In this model most of the flow goes through the transverse orifice.

The results for the IOP after glaucoma surgery are the following: in trabeculectomy, the IOP is equal to 7.1 mmHg while when using the EXPRESS™, IOP is 8 mmHg.

Finally, the glaucoma surgery has no effect on the shear stress of the iris surface compared to a normal case (figure 2-6C and 2-6D).

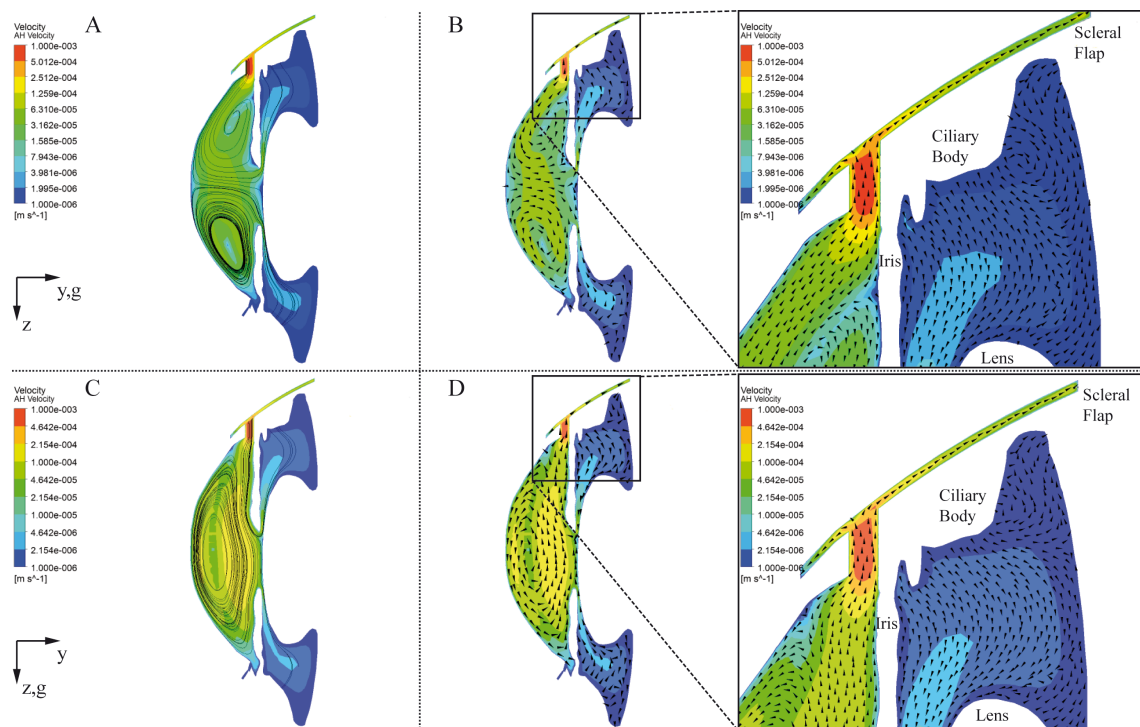


Figure 2-8: Contour of velocity magnitude and velocity vectors in anterior chamber in presence of a Trabeculectomy. $\Delta T = 2^\circ\text{C}$

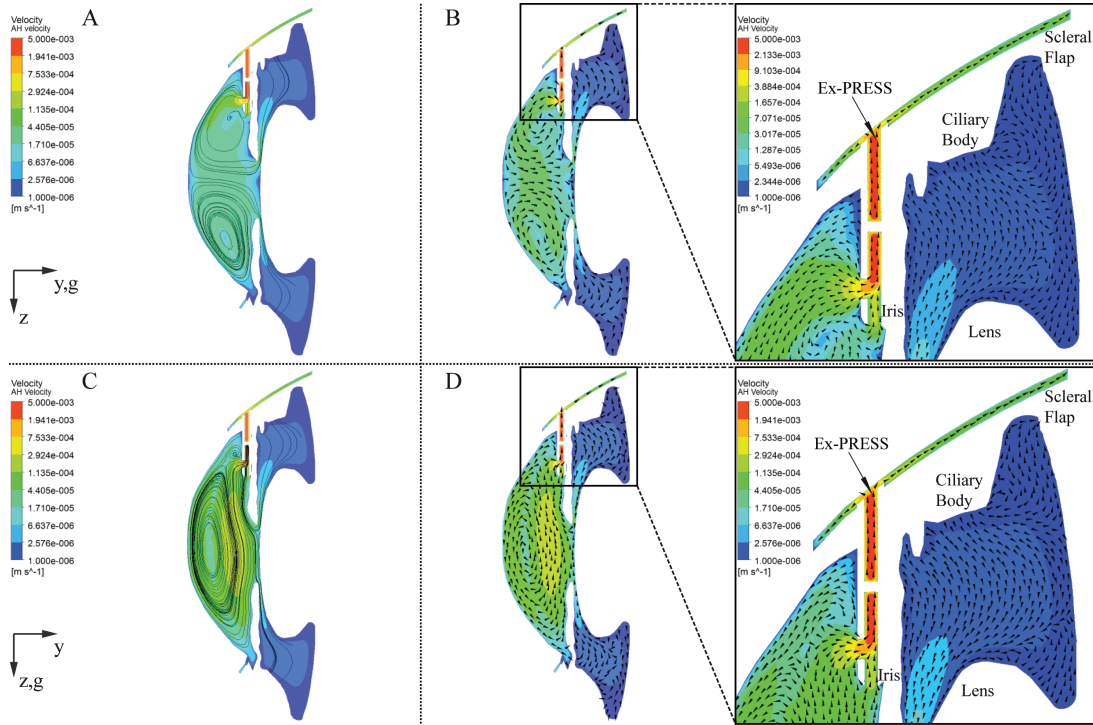


Figure 2-9: Contour of velocity magnitude and velocity vectors in anterior chamber in presence of an Ex-PRESS V50™ device. $\Delta T = 2^\circ\text{C}$.

2.4 Discussion

In this study we were interested in understanding the aqueous humor flow both in healthy eyes and in eyes undergoing glaucoma surgery. To achieve this goal, we have constructed a 3D model based on images from histology slides of a human eye. Dynamic characteristics in respect with velocity and pressure gradient along several drops of resistance have been depicted.

Schlemm's canal and TM contours were extracted from histology images. These structures are the most significant parts defining the AH flow resistance. Consequently special attention was given to their 3D reconstruction. Results of SC thickness were compared to those found by Irshad et al. [10], where the SC diameter was measured using Ultrasound Biomicroscopy *in vivo*. The average diameter values reported by Irshad and colleagues ($121 \pm 45 \mu\text{m}$) were lower than our results. Difference in results could possibly be due to disparities between *in vivo* and *in vitro* preparations.

The importance of buoyancy as the driving mechanism for AH flows has already been discussed previously [18]. Accordingly, we may consider that the orientation of the eye and the difference of temperature across the anterior chamber are the main driving mechanisms of AH in this region. In this study we have assumed a horizontal and a vertical upward-facing position of the human eye where the gravity direction is either perpendicular or parallel to the iris surface and the flow field is axi-symmetric. Under these conditions, the maximal velocity magnitude in the horizontal position is of the same order of magnitude as the maximum velocity found by Karampatzakis and Samaras [22] ($1.7 \times 10^{-5} \text{ m s}^{-1}$) for a 3D model of the eye. In the vertical position, the maximum velocity result found in this study is of the same order of magnitude and lies between the maximum velocities calculated by Heys and Barocas [14] ($0.7 \times 10^{-3} \text{ m s}^{-1}$) for a 3D model of the eye, Ooi and Ng [23] ($1.03 \times 10^{-4} \text{ m s}^{-1}$) for a 2D model of the eye and Karampatzakis and Samaras [22] ($3.36 \times 10^{-4} \text{ m s}^{-1}$). It is worth noting that in the Heys and Barocas and Ooi and Ng studies, the temperature of the corneal surface was kept constant at 34°C , whereas in the current study the temperature is higher, resulting in a smaller temperature gradient and consequently a lower velocity value.

In this study we have considered the TM as a volume with a constant determined permeability. Therefore it is represented by a porous structure with uniform resistance all over the filtration volume. However, in reality the human eye is made up of three layers with different porosity; the uveal meshwork, the corneoscleral meshwork and the juxtacanalicular or cribriform meshwork. The latter presents the highest resistance to AH egress [24]. In a previous study, Ethier et al. [13] described two possible structural models of the juxtacanalicular meshwork (JCM); a model A which represents JCM as a series of open spaces within a solid framework and a model B where the open channels are filled of a gel-like material. Murphy et al. [25] used these models to calculate the hydrodynamics properties of JCT. When using model A, they found the TM permeability for healthy patients ranged from 2 to $10 \cdot 10^{-15} \text{ m}^2$ while permeability varied between 2.9 and $3.4 \cdot 10^{-16} \text{ m}^2$ for patients suffering from open-angle

glaucoma. Our model is in agreement with these results. Nevertheless Murphy and colleagues found that the computed permeabilities from model A were much too high compared with the value they expected to achieve. For instance to match at best the experimental data we have a too large TM to build up a significant flow resistance unless it is filled with viscous material like in the model B. In the future, the structure of the TM and its complexity should be implemented in our model. Instead of having a uniform resistance represented by porous structures, the TM spaces and its different layers should include a gradient of porosity and it should be filled with a gel-like material to be consistent with the experimental data.

2.4.1 Wall shear stress

Wall shear stress studies are important for the investigation of endothelial cells' functions and structures [26]. In this model WSS was computed for the SC and the CCs and results could possibly be used to determine the biomechanical forces applied to Schlemm's canal endothelial cells. From that prospective, Ethier et al. [27] characterized the biomechanical environment of Schlemm's canal endothelial cells by estimating the average shear stress in SC. In their study, Ethier et al. showed that Schlemm's canal endothelial cells were exposed to a combination of shear stress and basal-to-apical pressure gradient resulting in different F-actin architectures. Using their calculations of the average shear stress upon the SC height, WSS at collector channel ostium is equal to $7 \cdot 10^{-3}$ Pa, which is of the same order of magnitude as the WSS computed in our model ($1.2 \cdot 10^{-2}$ and $9 \cdot 10^{-3}$ Pa). Differences are likely due to approximations made in the size of the SC in our model, which allowed fluctuations in its diameter.

The magnitude of the WSS on the iris surface is an important parameter for the prevision of endothelial cell detachment in Pigment Dispersion Syndrome and Pigmentary glaucoma [18, 28]. According to Gerlach [29] and colleagues, the magnitudes required to detach such cells are comprised between 0.51 and 1.53 Pa. In that respect, the comparison between the vertical

and the horizontal orientation of the iris and the corneal surfaces in our study demonstrated that the WSS results are lower than the values predicted to detach the endothelial cells. So it is unlikely that fluid shear stress could detach pigments from the anterior iris surface in our case. Nevertheless the probability and location of pigments detachment on the iris surface could be predicted using the plot of shear stress in case of some specific disease.

Further studies of shear stress in the eye involving different parameters could possibly be first tested with the present model. Results provided by the WSS simulations in this study support this idea.

2.4.2 Filtering surgery

The role of the glaucoma filtering surgery is to reduce IOP by increasing AH outflow. A retrospective comparison between trabeculectomy and an Ex-PRESS™ device inserted under a scleral flap showed the efficacy in lowering IOP for both surgeries [30]. With a follow-up of 3 months, the reduction of IOP was similar in both techniques. However, from day 1 to month 3 after surgery the IOP was significantly lower after trabeculectomy compared to the Ex-PRESS™ shunt implantation. This resulted in lower rates of early postoperative hypotony using the Ex-PRESS™ implant. Maris et al. [30] suggested that this difference was due to the additional resistance to AH flow provided by the smaller lumen of the Ex-PRESS™. In our study, resistance to AH outflow decreased and low IOP was established in the anterior chamber in presence of both procedures. In case of trabeculectomy, IOP was closer to the pressure of episcleral veins than in presence of the Ex-PRESS™ implant. Likewise Maris and colleagues found that the lumen of the device played a significant role in decreasing IOP in the anterior chamber.

Velocity streamlines using the Ex-PRESS™ tube demonstrated the importance of the lateral orifice to increase AH outflow. Results indicated that the resistor shaft inserted in the inner lumen is of major importance in contributing to the AH flow resistance. Such observations

were demonstrated by Broquet et al. [31]. In their study, they have made the same observations after similar simulation in ideal human eye geometry. Broquet and colleagues have shown that most of the resistance to AH egress through the device occurred at the level of the resistor shaft and most of aqueous humor flow occurred through the lateral orifice of the filtering device. Such simulations have supported the effectiveness of surgical interventions when AH flow resistance was high.

Finally fibrosis is believed to play an important role in the success of glaucoma surgery. In order to have a more realistic model, it is essential to create a time-varying fibrosis model where the resistance of outflow is changing over time. As such the scleral flap could be filled with a porous media representing the fibrotic tissue. Moreover the uveoscleral pathway has not been taken into account in this study. Previous studies have reported that the uveoscleral pathway can be in the range of 0.8 up to 1.0 $\mu\text{l}/\text{min}$ [32, 33]. While it does not account for an important part of the total AH outflow, it has been nevertheless reported that this pathway decreases significantly with age [32, 33]. Furthermore it was also shown that the uveoscleral drainage could be IOP dependent [34]. Such observations are interesting as age and pressure dependent changes in the uveoscleral pathway should be considered to enhance the accuracy of this model in the future.

2.5 Conclusion

We have presented a three-dimensional model of the human eye that could be used to investigate the pressure drop and the localization of the main resistance to aqueous egress.

Results of such simulations representing healthy and glaucoma eyes were consistent with previous 2D and 3D models based on ideal geometries. The addition of a filtering procedure showed a real diminution of the IOP.

Such model could help in determining the optimal placement and design of GDDs and glaucoma surgical techniques. However, some refinements still need to be done to improve precision and efficacy such as the addition of the uveoscleral pathway, remodeling TM and the implementation of a time-varying subconjunctival fibrosis after filtering surgery.

2.6 Acknowledgements

We are grateful to M. Broquet, M. Schmocker and to M. Alkharfane for providing structures of the synthetic eye and for scientific and mathematical advice.

The human eyes were obtained from the Cleveland Eye Bank, (OH, USA) and we thank the team for their contribution to this study.

2.7 References

- [1] Congdon N, O'Colmain B, Klaver CC, Klein R, Munoz B, Friedman DS, et al. Causes and prevalence of visual impairment among adults in the United States. *Arch Ophthalmol*. 2004;122:477-85.
- [2] Ethier CR, Johnson M, Ruberti J. Ocular Biomechanics and Biotransport. *Annual Review of Biomedical Engineering*. 2004;6:249-73.
- [3] Kwon YH, Fingert JH, Kuehn MH, Alward WL. Primary open-angle glaucoma. *N Engl J Med*. 2009;360:1113-24.
- [4] Chen PP, Yamamoto T, Sawada A, Parrish RK, 2nd, Kitazawa Y. Use of antifibrosis agents and glaucoma drainage devices in the American and Japanese Glaucoma Societies. *J Glaucoma*. 1997;6:192-6.
- [5] Joshi AB, Parrish RK, 2nd, Feuer WF. 2002 survey of the American Glaucoma Society: practice preferences for glaucoma surgery and antifibrotic use. *J Glaucoma*. 2005;14:172-4.
- [6] Schnyder C. *Glaucoma*. Paris: Elsevier; 2005.
- [7] Llobet A, Gasull X, Gual A. Understanding trabecular meshwork physiology: a key to the control of intraocular pressure? *News Physiol Sci*. 2003;18:205-9.
- [8] Bill A. Blood circulation and fluid dynamics in the eye. *Physiol Rev*. 1975;55:383-417.
- [9] Bill A, Phillips CI. Uveoscleral drainage of aqueous humour in human eyes. *Experimental Eye Research*. 1971;12:275-81.
- [10] Irshad FA, Mayfield MS, Zurakowski D, Ayyala RS. Variation in Schlemm's canal diameter and location by ultrasound biomicroscopy. *Ophthalmology*. 2010;117:916-20.
- [11] Flammer J. *Glaucoma : a guide for patients ; an introduction for care-providers ; a reference for quick information*. Bern: Huber; 2001.
- [12] Canning CR, Greaney MJ, Dewynne JN, Fitt AD. Fluid flow in the anterior chamber of a human eye. *IMA J Math Appl Med Biol*. 2002;19:31-60.
- [13] Ethier CR, Kamm RD, Palaszewski BA, Johnson MC, Richardson TM. Calculations of flow resistance in the juxtacanalicular meshwork. *Invest Ophthalmol Vis Sci*. 1986;27:1741-50.
- [14] Heys JJ, Barocas VH. A Boussinesq Model of Natural Convection in the Human Eye and the Formation of Krukenberg's Spindle. *Annals of Biomedical Engineering*. 2002;30:392-401.
- [15] Johnson MC, Kamm RD. The role of Schlemm's canal in aqueous outflow from the human eye. *Invest Ophthalmol Vis Sci*. 1983;24:320-5.
- [16] Scott JA. The computation of temperature rises in the human eye induced by infrared radiation. *Phys Med Biol*. 1988;33:243-57.
- [17] Scott JA. A finite element model of heat transport in the human eye. *Phys Med Biol*. 1988;33:227-41.
- [18] Kumar S, Acharya S, Beuerman R, Palkama A. Numerical Solution of Ocular Fluid Dynamics in a Rabbit Eye: Parametric Effects. *Annals of Biomedical Engineering*. 2006;34:530-44.
- [19] Cairns JE. Trabeculectomy. Preliminary report of a new method. *Am J Ophthalmol*. 1968;66:673-9.
- [20] Avtar R, Srivastava R. Modelling aqueous humor outflow through trabecular meshwork. *Applied Mathematics and Computation*. 2007;189:734-45.

- [21] Kocak I, Orgul S, Flammer J. Variability in the measurement of corneal temperature using a noncontact infrared thermometer. *Ophthalmologica*. 1999;213:345-9.
- [22] Karampatzakis A, Samaras T. Numerical model of heat transfer in the human eye with consideration of fluid dynamics of the aqueous humour. *Physics in Medicine and Biology*. 2010;55:5653-65.
- [23] Ooi E, Ng E. Simulation of aqueous humor hydrodynamics in human eye heat transfer. *Computers in Biology and Medicine*. 2008;38:252-62.
- [24] Johnson M. 'What controls aqueous humour outflow resistance?'. *Exp Eye Res*. 2006;82:545-57.
- [25] Murphy CG, Johnson M, Alvarado JA. Juxtacanalicular tissue in pigmentary and primary open angle glaucoma. The hydrodynamic role of pigment and other constituents. *Arch Ophthalmol*. 1992;110:1779-85.
- [26] Reneman RS, Arts T, Hoeks AP. Wall shear stress--an important determinant of endothelial cell function and structure--in the arterial system in vivo. Discrepancies with theory. *J Vasc Res*. 2006;43:251-69.
- [27] Ethier CR, Read AT, Chan D. Biomechanics of Schlemm's Canal Endothelial Cells: Influence on F-Actin Architecture. *Biophysical Journal*. 2004;87:2828-37.
- [28] Lehto I, Ruusuvaara P, Setälä K. Corneal endothelium in pigmentary glaucoma and pigment dispersion syndrome. *Acta Ophthalmol*. 1990;68:703-9.
- [29] Gerlach JC, Hentschel F, Spatkowski G, Zeilinger K, Smith MD, Neuhaus P. Cell detachment during sinusoidal reperfusion after liver preservation: an in vitro model. *Transplantation*. 1997;64:907-12.
- [30] Maris PJ, Jr., Ishida K, Netland PA. Comparison of trabeculectomy with Ex-PRESS miniature glaucoma device implanted under scleral flap. *J Glaucoma*. 2007;16:14-9.
- [31] Broquet J, Roy S, Mermoud A. Visualization of the aqueous outflow pathway in the glaucoma surgery by finite element model of the eye. *Computer Methods in Biomechanics and Biomedical Engineering*. 2005;8:43-4.
- [32] Toris CB, Yablonski ME, Camras CB, Gleason ML. Uveoscleral outflow decreases with age in ocular normotensive humans. *Invest Ophthalmol Vis Sci*. 1996;37:1909-.
- [33] Townsend DJ, Brubaker RF. Immediate effect of epinephrine on aqueous formation in the normal human eye as measured by fluorophotometry. *Invest Ophthalmol Vis Sci*. 1980;19:256-66.
- [34] Bill A. Further studies on the influence of the intraocular pressure on aqueous humour dynamics in cynomolgus monkeys. *Invest Ophthalmol Vis Sci*. 1967;6:364-72.

Chapter 3 : 2nd Paper

Published in IOVS, March 2014.

A New Adjustable Glaucoma Drainage Device

Adan Villamarin,¹ Sylvain Roy,^{1,2} Stéphane Bigler,¹ and Nikos Stergiopoulos¹

¹Laboratory of Hemodynamics and Cardiovascular Technology, Swiss Federal Institute of Technology, Lausanne

²Glaucoma Center Montchoisi Clinic, Lausanne, Switzerland

Invest Ophthalmol Vis Sci. 2014;55:1848–1852.

Doi: 10.1167/iovs.13-12626

Submitted: June 18, 2013

Accepted: February 10, 2014

3.1 Introduction

Glaucoma is one of the leading causes of blindness in the world ^{1,2} and lowering the intraocular pressure (IOP) to prevent optic nerve damage is one of the solutions to control glaucoma progression. Medication is the primary therapy used for patients suffering from glaucoma. However for some patients, pharmacological solutions may be inefficient and surgical procedure is required ³.

Several glaucoma-filtering techniques exist and most of them demonstrated efficacy in lowering IOP⁴⁻⁶. They all aim at decreasing the resistance to aqueous humor outflow by creating an additional flow pathway to the conventional ones. For several decades trabeculectomy ⁷ was one of the most frequently used surgical techniques. However, recent studies have shown a positive trend in the use of drainage devices in glaucoma surgery while the rate of trabeculectomy is decreasing ⁶. The increasing popularity of filtering devices can be attributed to the fact that IOP is reduced in a way that is associated with fewer side effects compared to established techniques⁸.

The Ex-PRESS mini shunt is a stainless steel implant inserted under a scleral flap, and the operation is similar to the trabeculectomy^{9,10}. Even if the rate of early hypotony has decreased using this kind of device compared to classic trabeculectomy, the rate of complications remained comparable¹¹⁻¹³. This implant aims at improving the way trabeculectomy works. However, as for all filtering procedures, the lack of proper IOP control can lead to post-surgical complications. Hypotony remains one of the main complications in the early steps post-surgery and a proper control of the IOP through the adjustment of the aqueous humor egress would probably help minimizing the occurrence of such post-operative complications.

In that prospect, the ideal filtering device should consist of an adjustable resistor valve that, upon proper adjustment, would take into account the post-operative hypotony and allows for customized adjustments of the IOP.

In this study we present the very first report of a novel adjustable glaucoma drainage device. Preliminary results from in vitro perfusion tests and ex vivo studies on enucleated eyes demonstrate that the model device is able to effectively and reproducibly control the resistance to aqueous humor (AH) egress.

3.2 Materials and Methods

3.2.1 Adjustable glaucoma drainage device

Figure 1 shows the adjustable glaucoma drainage device (AGDD) (Fig. 3-1A) and its external control unit (CU) (Fig. 3-1B), which is used to a) read the functional position of the implant and b) adjust its fluidic resistance. The concept of the adjustable glaucoma drainage device was first invented by Stergiopoulos¹⁴ and later developed and patented by Bigler and Stergiopoulos¹⁵. The AGDD is designed to drain aqueous humor with a resistance to outflow that can be externally regulated. The implant is inserted surgically under a scleral flap, in a manner similar to the Ex-PRESS shunt⁴. It is composed of a deformable silicone (MED-4830, Nusil, FL, USA) tube (outer diameter 0.3 mm, internal diameter 0.2 mm), which drains AH from the anterior chamber into a bleb formed in the scleral space. For a given rate of drainage, the IOP depends on the fluidic resistance of the tube. The implant contains a mechanism (Fig. 3-2), which allows for a variable compression of the tube, altering its cross-sectional area accordingly and thus changing the fluidic resistance. The various levels of compression in the tube are achieved by rotating a magnetic disk around a shaft, which is eccentric to its axis of symmetry. The angular position of the magnetic disk defines the length of the tube that is compressed as well as the degree of radial compression.

The external measurement/adjustment device, also termed as control unit (CU), is depicted in Figure 1B. The CU has been designed to help the physician perform two essential functions: a) measure the functional (angular) position of the implant, and b) perform a noninvasive adjustment of this functional position, in order to optimize the drainage characteristics (fluidic resistance) of the implant. The measurement of the angular position of the magnetic disk is performed with the use of a flat compass, which is situated in one of the two ends of the control unit. The magnetic needle is colored to indicate the “north pole” and the transparent cover slip or the outer rim of the compass housing contains graduations for easier reading of the angular position of the needle. The other extremity of the control unit contains a permanent magnet for performing the adjustment. To adjust the angular position of the implant, the operator first reads the actual angular position of the implant’s magnetic disk by placing the compass above of the implant (Fig. 3-3). Once the angular position is read, the operator flips the CU 180 degrees to bring the CU magnet in the vicinity of the implant, in order to couple magnetically the external magnet to the internal magnetic disk. The operator then drags the magnet in a clockwise or counterclockwise direction along a circular arc

around the implant, forcing thus the internal magnetic disk to rotate accordingly. The operator verifies the new angular position of the implant using the compass again.

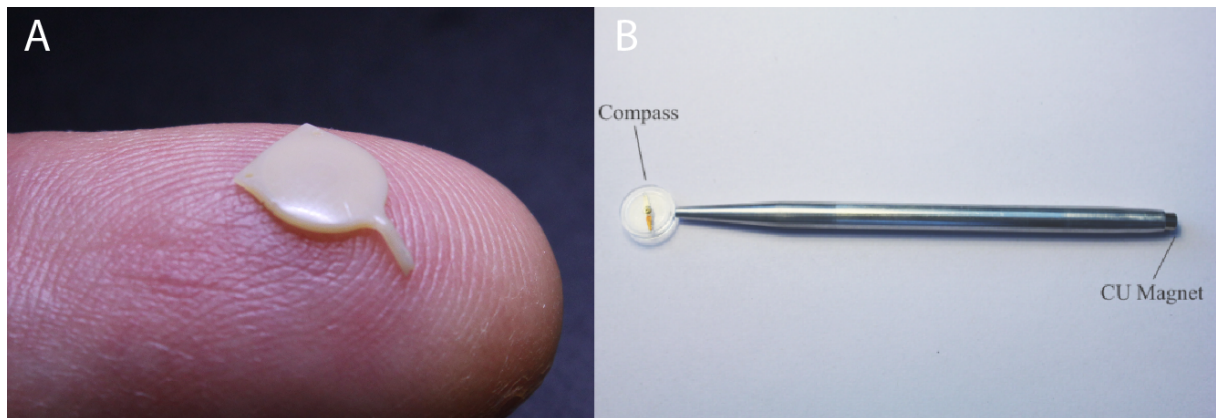


Figure 3-1: Picture of the Adjustable Glaucoma Drainage Device (A) and its Control Unit (B).

The mechanism (Fig. 3-2) and the tube of the AGDD are encapsulated within two shells made of synthetic polymer (PEEK Optima, Invibio, UK). These shells are hermetically shielded to protect the mechanism from tissue contact and fluid entry, which could jeopardize its functionality over time. The aqueous humor enters the tube through the nozzle and exits at the backside of the implant, totally shielded from implant's interior. To optimize the positioning of the device under a scleral flap, the shells and the mechanism have been designed to match the radius of curvature of the human eye.

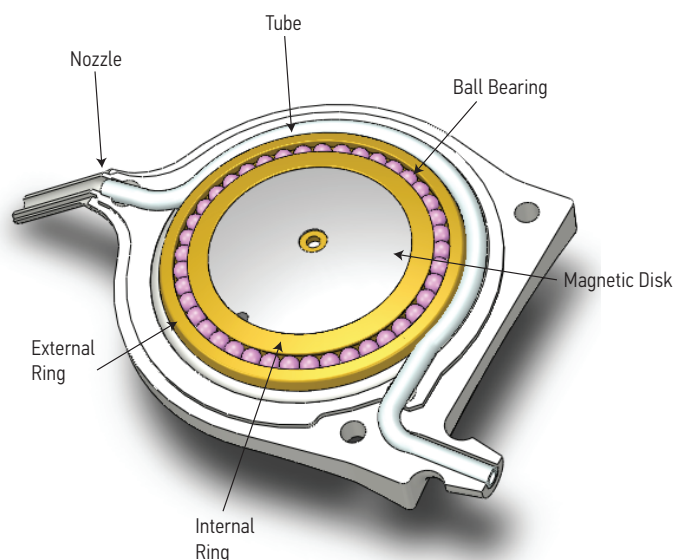


Figure 3-2: Synthetic image depicting the details of the mechanism of the AGDD. Under the steering effect of external magnetic fields, the magnetic disk of the implant turns around an eccentric axis pushing or retracting radially the external ring of the bearing ball mechanism. The radial motion of the external ring leads to a change of the cross-sectional area of the elastic tube, thereby modifying its fluidic resistance.

3.2.2 In vitro experimentation

The AGDD was connected to a syringe pump (SP210iw, World Precision Instruments, FL, USA) pushing through the implant's tube saline solution at a rate of 2 $\mu\text{L}/\text{minute}$. The saline solution would flow out of the distal end of the tube into the atmosphere. Pressure upstream of the implant was measured with an electronic manometer (BLPR2, World Precision Instrument, FL, USA). The manometer was connected to a data acquisition card (DAQPad-6015, National Instruments, TX, USA) to give real-time pressure readings via a custom interface (LabView 9.0, National Instruments, TX, USA).

The angular position of the implant was changed using the CU. The magnet's angular position was adjusted from 0° to 180° (in 5° steps) and the steady-state pressure was recorded at each position. Three sets of data of pressure vs. angular position were obtained for each implant. Experiments were conducted on 6 different implants.

3.2.3 Ex vivo experimentation

Six freshly enucleated eyes (post-mortem time less than 4 hours) from white New Zealand rabbits were obtained from a local farm. The eye was held on a brace, and the anterior chamber was cannulated with a 24-gauge catheter (Optiva W, Smiths Medical, Rossendale, UK) filled with saline solution that was delivered by a syringe pump at a rate of 20 $\mu\text{L}/\text{min}$ during the experimentation. The catheter was inserted between the anterior plane of the iris and the posterior surface of the cornea. The system was connected to an electronic manometer and real-time pressure reading and recording were performed as for the in vitro experiment, after implanting the device. The angular positions of the magnetic disk were adjusted from 0 to 180° at intervals of 5° .

3.2.4 Surgical procedure

The eye was maintained on the mounting unit and a 24-G canula (Optiva W, Smiths Medical, Rossendale, UK) was inserted in the anterior chamber. The canula was connected to a water column containing saline solution, so that physiological ocular rigidity was maintained throughout the surgery. The height of the column was set to pressurize the eye at 25 mmHg. A square scleral flap, 7×7 mm, was cut using a crescent sapphire blade down to 1 mm from the limbus. A 24-G needle was then used to poke the scleral wall and to enter the anterior chamber, creating a hole for entering the device's nozzle into the anterior chamber. Because the nozzle was inserted in the space between the cornea and the anterior surface of the iris, care was taken not to touch either of these structures. The implant was secured using 2 single

Nylon 10-0 sutures, and the scleral flap was repositioned and sutured using 2 single point Nylon 10-0. Finally, the 24-G canula was connected to the syringe pump delivering 20 $\mu\text{L}/\text{minute}$, which deemed necessary to maintain IOP above 21 mmHg.

3.2.5 Outflow facility measurement

Details of outflow facility measurement have been reported previously^{16,17}. Briefly, the anterior chamber was perfused at first with a defined flow rate (2 $\mu\text{L}/\text{minute}$). After a stable IOP level was reached, the flow rate was changed to a higher value until another stable IOP level was reached. The outflow facility (OF) was then calculated using the Goldman equation

$$OF = \Delta Q / \Delta IOP \quad (\Delta Q = (Q_2 - Q_1))$$

where Q_1 and Q_2 are successive inflow rates ($\mu\text{L}/\text{minute}$), $\Delta Q = Q_2 - Q_1$ and $\Delta IOP = (P_2 - P_1)$, with P_1 and P_2 representing IOP at Q_1 and Q_2 , respectively (mmHg).

3.2.6 Statistics

The results were expressed as the mean and standard deviation (mean \pm SD). The paired Student's t-test was used to assess significant differences in angular position adjustments on the results. $P < 0.05$ was considered statistically significant.

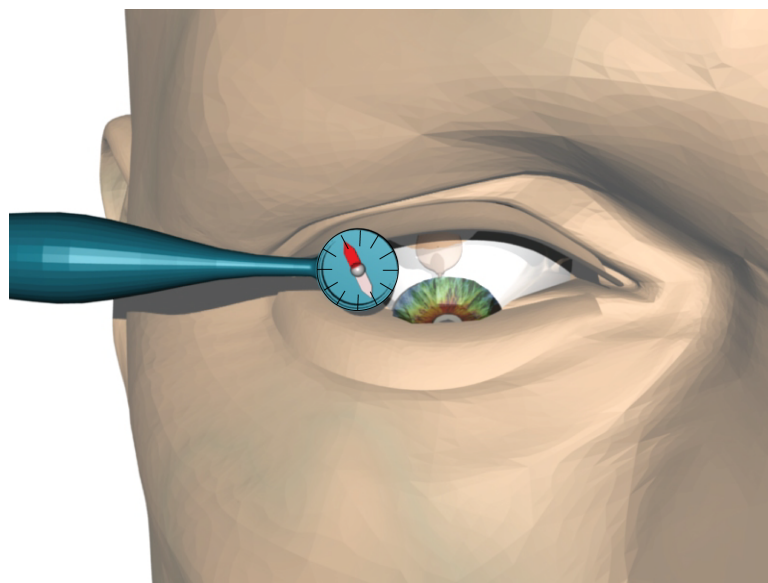


Figure 3-3: Synthetic image showing the positioning of the implant within the scleral flap and the compass of the CU, which is used to read out the angular orientation of the implant's magnetic disk. The operator may adjust the angular position of the implant using the CU magnet.

3.3 Results

3.3.1 In vitro experimentation

The relationship between the pressure drop and the adjustment is non-linear (Fig. 3-4). From position 0° to 80° the resistance of the tube is equal or close to 0 ($p = 0.2$) meaning the AGDD configuration is fully open. From position 120° and higher the pressure drop is high (> 30 mmHg) and adjustments become less accurate.

Significantly different pressure drops may be achieved every 10° ($\Delta\theta$) from 90° to 130° ($p < 0.05$). Under 10° steps differences in pressure are no more statistically significant. This means that the angular resolution of the device is approximately 10°.

The resistance of the AGDD to aqueous outflow when totally open (position 0°) is equal to 0.05 mmHg·minute/ μ L.

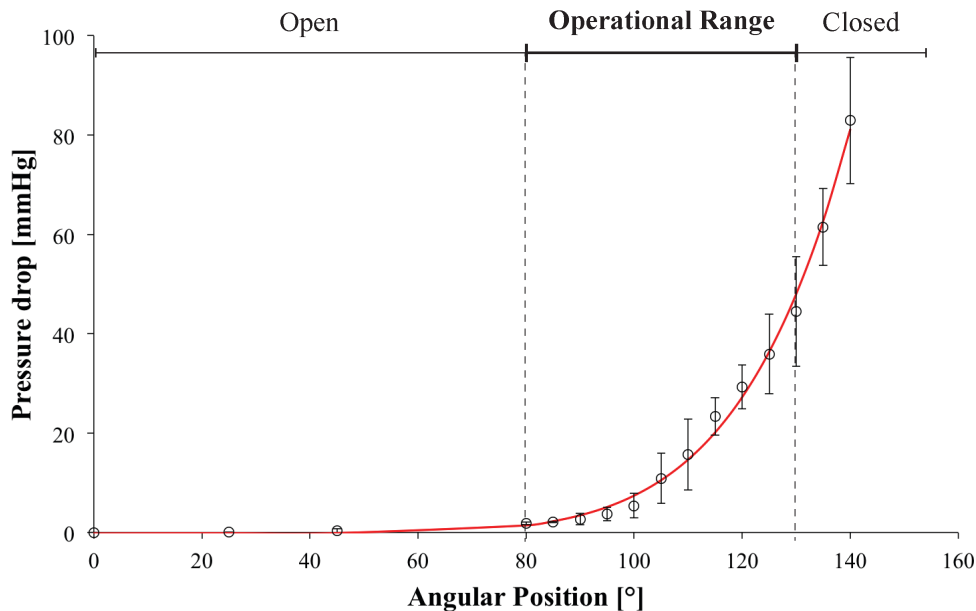


Figure 3-4: In vitro measurements of the pressure drop vs. the angular position of the magnetic disk. The operational range is comprised between 80° and 130°. Values are given as average \pm standard deviations ($n = 6$). The operational range of the device is defined as the angular range between its fully closed and fully open position. The fitted curve corresponds to a power law: $f(x) = a \cdot x^b + c$, where $a = 4.81 \cdot 10^{-14}$, $b = 7.056$ and $c = -0.15$. $R^2 = 0.99$.

3.3.2 Ex vivo experimentation

The outflow facility before surgery was 0.33 ± 0.09 μ L/mmHg/minute and 1.27 ± 0.19 after implantation ($p < 0.05$). To maintain high pressure in the eye, the flow rate was increased to 20 μ L/minute resulting in an IOP of 23 ± 2.5 mmHg when the implant was in a fully closed position.

The angular position of the AGDD was adjusted in steps of 5 degrees and the IOP at the new steady state was recorded (Fig. 3-5). The IOP range from the fully closed to fully open position ranged from 23 ± 2.5 to 3.7 ± 0.7 mmHg ($p < 0.05$).

IOP vs angular position curves from in vitro and ex vivo measurements (Fig. 3-4 and 3-5) were fit with an empirical power law ($y = a \cdot x^b + c$). The corresponding values were: $b = 7.056 \pm 0.706$ for in vitro and $b = 7.004 \pm 1.297$ for the ex vivo experimentation, demonstrating, as expected, an identical exponent in the power law for the in vitro and ex vivo experiments.

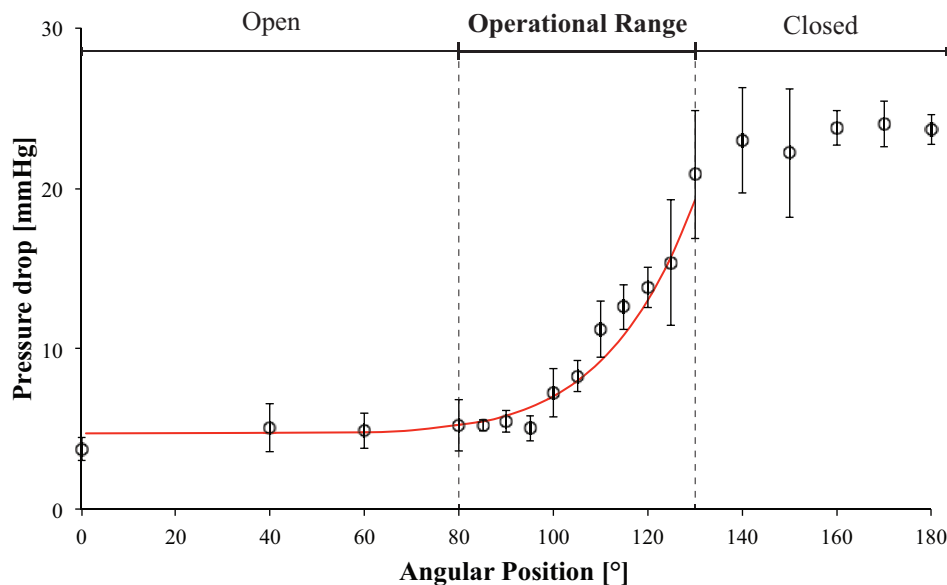


Figure 3-5: Ex vivo measurements of the pressure drop as function of the angular position of the magnetic disk. The implant was surgically placed in its intended anatomical position under a scleral flap in enucleated rabbit eyes. Values are given as average \pm standard deviations ($n = 6$). The operational range of the device is defined as the angular range between its fully closed and fully open position. The fitted curve corresponds to a power law: $f(x) = a \cdot x^b + c$, where $a = 2.26 \cdot 10^{-14}$, $b = 7.004$ and $c = 4.739$. $R^2 = 0.98$.

3.4 Discussion

In this study, we have tested a new experimental adjustable glaucoma drainage device, which allows for a non-invasive and non-traumatic adjustment of the fluidic resistance of the shunt, thereby offering a customized control of intraocular pressure. The present in vitro and ex vivo experiments are the first steps to validate the fluidic characteristics and performance of this new implant. Results show that the drainage device described in this study can be adjusted by varying the angular position of the disk using an external magnet, thus modifying the cross-section area of the draining tube and changing its fluidic resistance. The resistance may vary from infinite (fully closed position) to a minimal value (fully open position), allowing the user to select over a wide range of IOPs.

The working range for the angular position of the implant is situated between 80° and 130°. Angular positions outside of this range correspond to fully open ($\theta \leq 80^\circ$) or fully closed configurations ($\theta \geq 130^\circ$). Within this working range and given the fact that the angular resolution is in the order of 10°, there are effectively 4-5 distinctly different positions that the user can select with good confidence in order to alter the resistance. This means that there is not only a binary system (open/closed) configuration, but there is also the possibility to selectively set the resistance of the implant, and thus adjust IOP in accordance to the different patient needs.

The pressure drop across the implant for a given flowrate is non-linearly related to the angular position of the implant's disk. The angular position of the magnetic disk of the implant defines the degree of compression of the elastic tube, which defines the internal cross-sectional area of the tube and thus its fluidic resistance. According to Poiseuille's law, the hydraulic resistance (RH) to flow is inversely proportional to the radius (r) of the tube to the power 4 ($RH \propto (1/r^4)$). Thus when the hydraulic inner radius of the tube becomes smaller (due to compression by the magnetic disk), the resistance increases by the power of 4, e.g. a reduction by half of the diameter leads to a 16 times increase of the resistance. For the particular implant design, the degree of compression is non-uniform along the tube and it is nonlinearly dependent of the angular position θ . An empirical fit of the pressure drop vs. angular position of the magnetic disk shows that pressure drop is proportional to the angle of adjustment to the seventh power. The resistance has therefore a very strong non-linear dependence on the angular position of the disk. The non-linearity of the system might be a limitation, as it reduces the number of adjustment points, making the system very sensitive to the angular position. An ideal system would exhibit a linear adjustment of the resistance as function of the angle of the disk. In that case, the angular working range would be greater and the angular precision on the adjustment would be less stringent.

During the ex-vivo experiments, eyes were artificially maintained at a pressure above 21 mmHg to mimic glaucoma conditions. High flow rates were used to stabilize IOP at such high level. This is mainly due to higher outflow facility of cadaveric eyes and to leakages occurring all around the insertion point of the implant's nozzle. The tests on the enucleated eyes demonstrated the efficacy and reproducibility of the AGDD to decrease IOP at various levels, depending on its angular position. Minimal pressures reached after total opening of the AGDD were slightly higher than zero due to high flow rates used in these experiments.

Based on these laboratory investigations, we plan to test the AGDD on an experimental animal model to confirm these initial results and to further evaluate the biocompatibility, the controllability and the efficacy of such device implanted in a living eye. The ultimate goal will be to conduct a clinical trial on patients suffering from medically uncontrolled glaucoma requiring a filtering procedure. In that prospect, the fine-tuning of the AGDD would be performed post-operatively according to the IOP measurements. For instance, if the IOP were too high (i.e., above 20 mmHg), the clinician would set the position of the magnetic disk of the AGDD in a new orientation to decrease its fluidic resistance and thus lower IOP. Conversely if the IOP is too low (i.e., below 5 mmHg, for instance), the clinician could modify the orientation of the disk to increase the resistance to aqueous egress, resulting in an increase of the IOP. In the early post-operative period, and when hypotony is present, the operator could set the AGDD in a fully closed position that would help increasing the IOP, thus contributing to minimize the problem of persistent post-operative hypotony and potentially decreasing the complications related to hypotony. The above envisioned scenario is speculative and needs to be verified through in vivo experiments in animals and in appropriately designed clinical studies.

In conclusion, this study demonstrates that the resistance to AH egress can be selectively changed with an adjustable glaucoma drainage device. This device provides various outflow resistances, which can be adjusted to bring IOP to clinically acceptable values. The adjustment can be performed simply and non-invasively using an external control unit. The in vitro results presented here need to be confirmed in vivo on the animal and on the human. Specifically, critical aspects, which cannot be studied in vitro, such as the biocompatibility, complications related to filtration, overall safety and the efficacy of the AGDD, will be investigated on an animal model before proceeding to a pilot human trial. The simplicity of the device, the relative ease with which resistance is adjusted over a wide range and the standard way of implanting allow us to hypothesize that this first ever adjustable glaucoma drainage device may prove to be a valuable tool in the surgical treatment of glaucoma.

3.5 Acknowledgments

We are grateful to A. Mermoud for his scientific advice.

Disclosure: A. Villamarin, None; S. Roy, None; S. Bigler, None; N. Stergiopoulos, None

3.6 References

1. Congdon N, O'Colmain B, Klaver CC, et al. Causes and prevalence of visual impairment among adults in the United States. *Arch Ophthalmol*. 2004;122:477–485.
2. Quigley HA, Broman AT. The number of people with glaucoma worldwide in 2010 and 2020. *Br J Ophthalmol*. 2006;90:262–267.
3. Ramulu PY, Corcoran KJ, Corcoran SL, Robin AL. Utilization of various glaucoma surgeries and procedures in Medicare beneficiaries from 1995 to 2004. *Ophthalmology*. 2007;114:2265–2270.
4. Bissig A, Feusier M, Mermoud A, Roy S. Deep sclerectomy with the Ex-PRESS X-200 implant for the surgical treatment of glaucoma. *Int Ophthalmol*. 2010;30:661–668.
5. Topouzis F, Coleman AL, Choplin N, et al. Follow-up of the original cohort with the Ahmed glaucoma valve implant. *Am J Ophthalmol*. 1999;128:198–204.
6. Desai MA, Gedde SJ, Feuer WJ, Shi W, Chen PP, Parrish RK, 2nd. Practice preferences for glaucoma surgery: a survey of the American Glaucoma Society in 2008. *Ophthalmic Surg Lasers Imaging*. 2011;42:202–208.
7. Cairns JE. Trabeculectomy. Preliminary report of a new method. *Am J Ophthalmol*. 1968;66:673–679.
8. Kersey T, Clement CI, Bloom P, Cordeiro MF. New trends in glaucoma risk, diagnosis & management. *The Indian journal of medical research*. 2013;137:659–668.
9. Dahan E, Carmichael TR. Implantation of a miniature glaucoma device under a scleral flap. *J Glaucoma*. 2005;14:98–102.
10. Ahmed I, Rai, SR. Ex-PRESS Glaucoma Filtration Device: Theory, Technique and Results. *Journal of Emmetropia*. 2013;4:104–114.
11. de Jong LA. The Ex-PRESS glaucoma shunt versus trabeculectomy in open-angle glaucoma: a prospective randomized study. *Adv Ther*. 2009;26:336–345.
12. Stein JD, McCoy AN, Asrani S, et al. Surgical management of hypotony owing to overfiltration in eyes receiving glaucoma drainage devices. *J Glaucoma*. 2009;18:638–641.
13. Seider MI, Rofagha S, Lin SC, Stamper RL. Resident-performed Ex-PRESS shunt implantation versus trabeculectomy. *J Glaucoma*. 2012;21:469–474.
14. Stergiopoulos N. Non-invasively adjustable drainage device. *US Patent*. 2011;12:742–955.
15. Bigler S, Stergiopoulos N. Apparatus and methods for treating excess intraocular fluid. *US Patent*. 2012;13:349–353.
16. Nguyen C, Boldea RC, Roy S, Shaarawy T, Uffer S, Mermoud A. Outflow mechanisms after deep sclerectomy with two different designs of collagen implant in an animal model. *Graefes Arch Clin Exp Ophthalmol*. 2006;244:1659–1667.

17. Villamarin A, Roy S, Stergiopoulos N. Eye vessel compliance as a function of intraocular and arterial pressure and eye compliance. *Invest Ophthalmol Vis Sci.* 2012;53:2831–2836.

Chapter 4 : 3rd Paper

Submitted to IOVS, April 2014.

In vivo testing of a novel adjustable glaucoma drainage device

Villamarin Adan¹, Stergiopoulos Nikos¹, Stéphane Bigler¹, Mermoud André², Moulin
Alexandre³, Roy Sylvain^{1,2}

¹Swiss Federal Institute of Technology, Lausanne, ²Glaucoma Center Montchoisi Clinic,
Lausanne, Switzerland, ³Jules Gonin Eyes Hospital, Lausanne, Switzerland

4.1 Introduction

Glaucoma is a leading cause of blindness affecting millions patients worldwide^{1,2}. Decreasing the intraocular pressure (IOP) is one of the most important requirements to efficiently control the progression of glaucoma³. The number of valuable options in glaucoma filtering surgery has increased over the last decade^{4,5}. Trabeculectomy and the use of implantable drainage devices or stents are parts of the armamentarium available nowadays in modern glaucoma filtering procedures. Glaucoma drainage implants become increasingly popular because they may offer better IOP control overtime, reducing the number of post-operative complications⁶.⁷ Still, predicting postoperative IOP and maintaining it at optimal levels remains a key problem. For instance, the risk of early post-operative complications, such as hypotony, is always present. Hypotony could entrain complications requiring further surgeries^{8,9}. In that respect, the possibility to control of the fluidic resistance of an implanted drainage device during the post-operative follow-up would have been very helpful in maintaining IOP always at optimal levels, thereby potentially avoiding a number of complications related to poor pressure control.

Recently, a new experimental non-invasively adjustable glaucoma drainage device (AGDD) has been developed¹⁰. In vitro results demonstrated that the fluidic resistance of the device can be adjusted to consequently regulate the IOP. In order to assess the safety and the efficiency of the novel device, this study reports the first *in vivo* testing of this AGDD.

4.2 Methods and Materials

The principle of the AGDD system was first described by Stergiopoulos¹¹, further developed and patented by Bigler and Stergiopoulos¹² and described in details by Villamarin et al.¹⁰. Briefly, the system comprises of a) the AGDD implant and b) the external measurement/adjustment device, hereafter called the control unit (CU) (Fig. 4-1). The AGDD contains a simple mechanism, which allows for a selective compression of an incorporated

drainage tube, thereby adjusting its fluidic resistance. This is achieved using the combination of an eccentrically placed magnetic disk (that is placed on ball bearings facilitating its rotation) and a ring compressing the silicone tube; the angle of rotation thus determines the amount of compression of the drainage tube, and therefore its fluidic resistance. The magnetic disk is rotated using the CU, which contains a magnet at one end and a compass on the other end. When placed on top of the implanted AGDD, the compass indicates the actual rotational position of the magnetic disk. The magnet is used to rotate the magnetic disk, by appropriately dragging the magnet along the periphery of the implant in the clockwise or counterclockwise direction. Both the reading (compass) and the adjustment (magnet) of the rotational position of the implant is done non-invasively and without even touching the eye (Fig. 4-1).

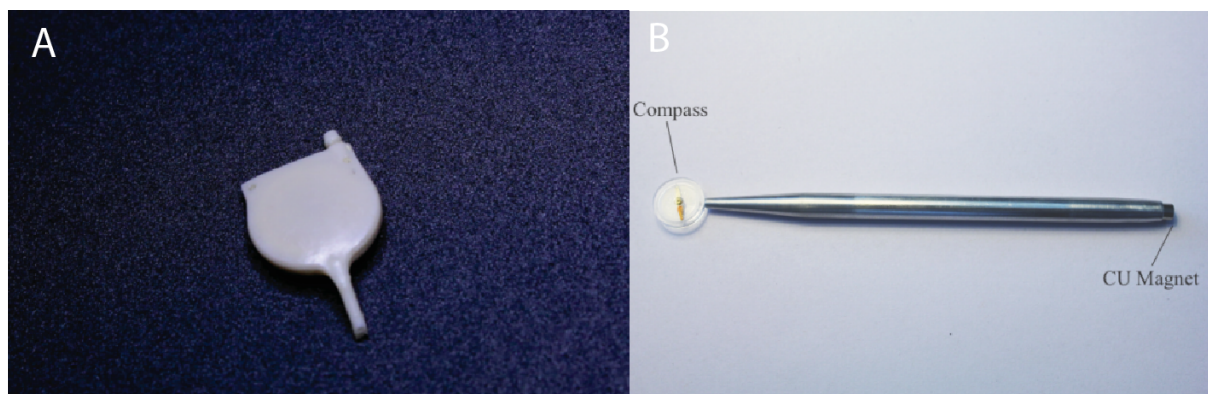


Figure 4-1: Picture of the AGDD (A) and the Control Unit (B) used for the measurement and the adjustment of the outflow resistance.

4.2.1 *In vivo experiment*

The study was carried out on 7 white New-Zealand rabbits for duration of 4 months. General anesthesia was performed using a mixture of 3 mg/kg (body mass) xylazine and 35 mg/kg ketamine intramuscular injection. Under general anesthesia, the AGDD was implanted in a way analogous to the Ex-PRESS® device¹³. In short, a scleral flap of 7x7 mm (width x long) was dissected and the nozzle was inserted in the anterior chamber between the cornea and the anterior surface of the iris taking care not to touch either of these structures (Fig. 4-2). The AGDD was implanted in a functionally closed position and left in that position during the

initial postoperative period (1 month). The end portion of the tube was placed freely under the conjunctiva and aqueous humor was drained in the subconjunctival space.

During the first postoperative week, IOP was measured daily on both the operated and the control eyes using a rebound tonometer (iCARE Tonovet, iCare, Finland). In the following weeks, such measurement was performed once a week. Results were reported and compared for statistics. Before each measurement, rabbits were placed in a bunny snuggle (Colonial Medical Supply, NH, US) and relaxed for 5 minutes. All measurements were performed at the end of the morning (10 a.m. to 12 a.m.).

Once a month the AGDD was adjusted non-invasively with the CU from its fully closed position to its fully open position and the resulting pressure drop was measured. Hypotony was defined as an IOP equal or lower than 6 mmHg ($IOP \leq 6$ mmHg). The contralateral eye was not operated and served as control. At the end of the study the animals were sacrificed and the eyes were enucleated to perform histology in order to assess the biocompatibility of the AGDD.

All experiments conformed to the ARVO Statement for the Use of Animals in Ophthalmic and Vision Research, and were reviewed and approved by the institutional committee for animal studies in Lausanne, Switzerland.

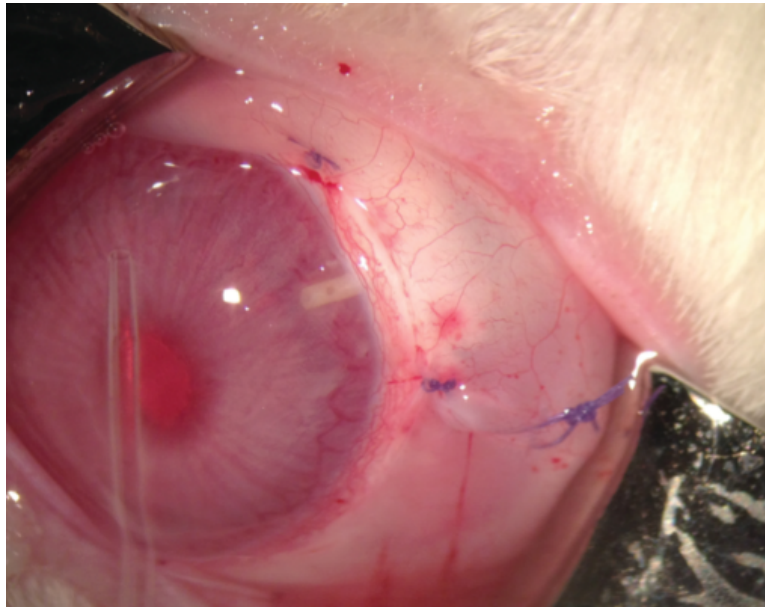


Figure 4-2: Picture of a rabbit eye where the AGDD was placed under a scleral flap with its nozzle inserted in the anterior chamber.

4.2.2 Histology

The enucleated eyes were formalin-fixed, macroscopically processed, and dehydrated through graded alcohol followed by paraffin inclusion. Five μm sections were cut and the following stains performed: Hematoxylin-Eosin, and Prussian Blue.

4.2.3 Statistics

The results were expressed as the mean and SD. The paired Student's t-test was used to assess significant differences and effects of the AGDD on the results. $P < 0.05$ was considered statistically significant.

4.3 Results

The mean preoperative IOP was 11.1 ± 2.4 mmHg. The evolution of IOP during the entire post-operative period for the animals is shown in Figure 3. For the 7 rabbits, hypotony was present in the operated eyes during the first 3 days after implantation (mean IOP was 6 ± 1.4 mmHg) and the difference with the control (non-operated) eyes was significant ($p < 0.05$). Eight days after surgery, hypotony was no longer present (mean IOP 11.3 ± 0.8 mmHg) and the difference in IOP between control and operated eyes was no longer significant ($p = 0.12$)

(Fig. 4-3). In all rabbits, the IOP dropped significantly from 11.2 ± 2.9 mmHg down to 4.8 ± 0.9 mmHg ($p < 0.05$) when the AGDD was opened from its fully closed (maximum outflow resistance) to fully opened (minimum outflow resistance) position (Fig. 4-4). The range of IOP from the closed position to the open position of the implant corresponds to [closed min=7 mmHg, max=17 mmHg] and [open min=4 mmHg, max 7 mmHg]. The pressure drop was significant for all rabbits ($p < 0.05$) and it was reproducible from one rabbit to the other.

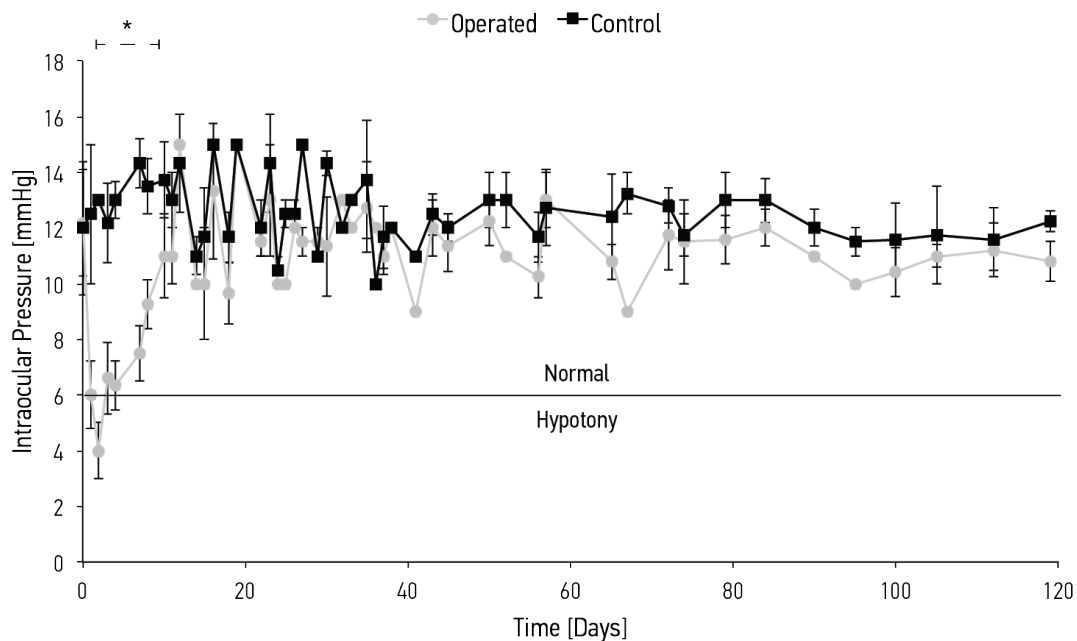


Figure 4-3: Plot of the IOP over time. Measurements were done every week with an iCARE TonoVet. Post-operatively the difference between the operated and the control eyes was significant from day 1 to day 8 (*). Transient hypotony was present in the operated eyes during the first 3 days after implantation.

Microscopic examination of tissues surrounding the AGDD showed a cavity covered by a layer flattened macrophages surrounded by partially reorganized dense connective tissue. In some areas, aggregates of lymphocytes as well scarce eosinophils could be identified. The chronic inflammatory infiltrate was minimal and mild in most of the cases (Fig. 4-5). A granulomatous foreign body type reaction was observed around the suture material.

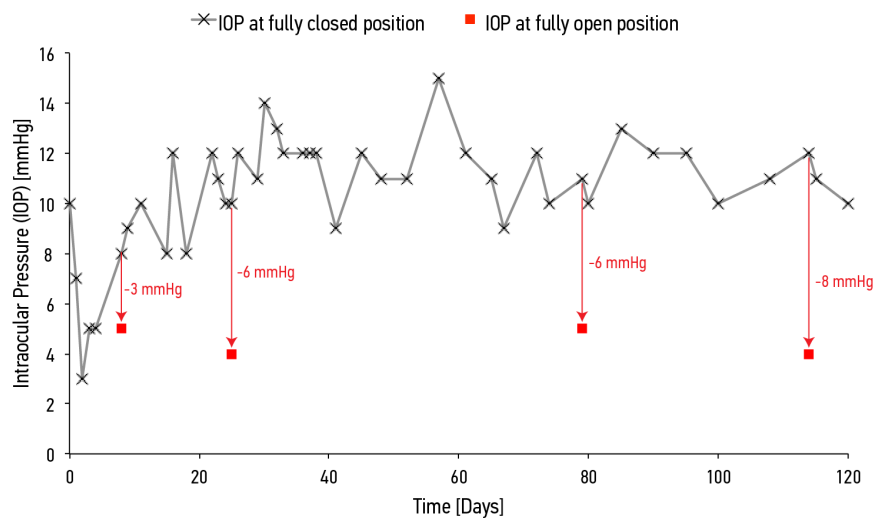


Figure 4-4: Plot of the IOP over time and the AGDD in its functionally closed position. Once a month, the AGDD was fully opened and the resulting pressure was measured (red square symbol). The arrows help visualizing the magnitude of the pressure drop when the device was adjusted from its fully closed to its fully opened position.

4.4 Discussion

The advantage of the novel glaucoma drainage device resides in the possibility to adjust, non-invasively, its fluidic resistance to the aqueous humor drainage. In that prospect, the goal of this study was to demonstrate the safety, efficacy, ease of use and biocompatibility of the AGDD in an animal model.

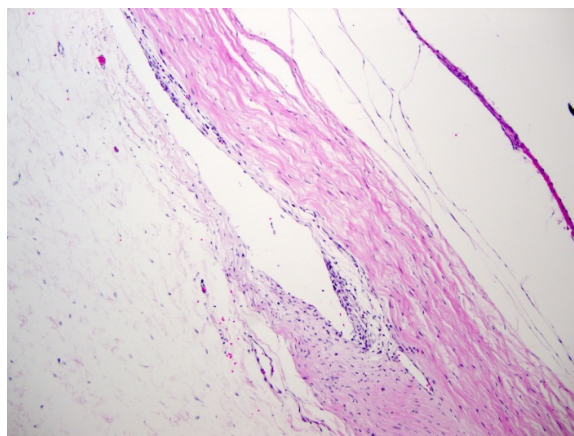


Figure 4-5: Histopathological analysis demonstrated a cavity lined by flattened cells surrounded by few lymphocytes. Circumscribed post surgical cicatricial remodeling can be observed inferior to the cavity in the dense connective tissue of the sclera. Original magnification: x 63; stain: Hematoxylin-Eosin.

Although rabbits are standard animal models commonly used in ophthalmology research¹⁴, the size of the rabbit eye is significantly smaller than humans. However, the anatomical structures are comparable, providing a useful surgical model for ophthalmic investigations¹⁵.

The rabbits used in this study did not suffer from glaucoma. It is rather difficult to induce glaucoma on rabbit eyes and to maintain an elevated IOP over time. Several techniques such as injection of microbeads into the anterior chamber¹⁶ or occlusion of episcleral vessels^{17, 18} can be effective but do not work for long-term follow-ups. In addition, these techniques were tried on rodents such as mice or rats that have too small eyes for the implantation of the AGDD. Therefore, the capability in reducing elevated IOP to normal range (as it would be the case for patients suffering from glaucoma) could not be tested in this study. However, the ability of the AGDD to reduce pressure levels (from normal to low pressures) has been clearly demonstrated. Because the implant operates on altering the fluidic resistance, one could imagine that in presence of glaucomatous eyes, the IOP could be reduced to pressures down to physiological range. Results show that the implant has efficiently decreased the IOP once it was in its functionally open position. These results demonstrate that over time the AGDD can be adjusted non-invasively and consequently the IOP can be adjusted accordingly. When the implant was re-adjusted from the fully open to its fully closed position, the following day, the IOP resumed its initial level (Fig. 4-4). These observations are very encouraging, demonstrating the efficacy of the implant to change the IOP and to customize the intraocular pressure specifically thinking to the needs of the patients. Nonetheless, further investigations are needed to clinically address elevated IOP in glaucoma patients.

The surgical method to implant the AGDD is analogous to the Ex-PRESS tube, which is comparable to the trabeculectomy technique¹⁹. Nevertheless, some minor changes were necessary to correctly implant the AGDD. For instance, the size of the scleral flap was substantially larger (7mm x 7mm) to correctly fit the size of the AGDD.

Results show that after a week (8 days, Fig. 4-3) the difference in IOP between control and operated eyes was no longer significant. For the eyes implanted with the AGDD, the IOP went back to preoperative level after only a few days following surgery and the hypotony was

thus minimized (< 4 days). This short recovery time after a filtering procedure results from the fact that the AGDD was inserted in its functional closed position thus limiting outflow to the leakages around the nozzle and allowing the eye to resume the initial IOP level. However, one should consider the increase in resistance resulting from the postoperative scarring of the rabbit eye²⁰. In humans, scarring would certainly have a different time profile and the control of optimal IOP pressure would be achieved by tuning the fluidic resistance of the implant following the fibrosis of surrounding tissue and the overall scarring response. The 4 months follow-up may be too short to fully evaluate the mid- to long-term safety and efficacy profile of this AGDD. This is the main limitation of this study. Further clinical evaluations are planned to address these issues.

The use of this AGDD as a modular flow resistance is most efficient in the early stages after implantation. Later on the function of the device would be to drain out the aqueous humor in a way analogous to standard drainage devices. Following the surgical procedure the AGDD could be set into a functional closed position to minimize hypotony. Once the clinically relevant IOP is reached, the resistance to outflow could be adjusted accordingly. Critical aspects such as safety and efficiency of the AGDD were assessed in this first in vivo study. The rate of aqueous humor outflow was easily adjustable during the entire postoperative period based on the control of the outflow resistance of the AGDD between the fully closed and fully open positions. The surgical technique to implant the AGDD is comparable to the Ex-PRESS® procedure, demonstrating the simplicity and relative ease of use of the implant. These first in vivo results provided encouraging data on the safety and performance of the device. A human clinical trial will follow to demonstrate all aspects of safety, performance and efficacy of the AGDD in glaucoma patients. This will provide an effective means of controlling IOP during the initial post-op period on a per patient basis, in the aim to possibly minimizing the risk of hypotony in the early postoperative stages and to offer optimal IOP control during the entire post-operative period.

4.5 References

1. Congdon N, O'Colmain B, Klaver CC, et al. Causes and prevalence of visual impairment among adults in the United States. *Arch Ophthalmol* 2004;122:477-485.
2. Quigley HA, Broman AT. The number of people with glaucoma worldwide in 2010 and 2020. *Br J Ophthalmol* 2006;90:262-267.
3. Ramulu PY, Corcoran KJ, Corcoran SL, Robin AL. Utilization of various glaucoma surgeries and procedures in Medicare beneficiaries from 1995 to 2004. *Ophthalmology* 2007;114:2265-2270.
4. Joshi AB, Parrish RK, 2nd, Feuer WF. 2002 survey of the American Glaucoma Society: practice preferences for glaucoma surgery and antifibrotic use. *J Glaucoma* 2005;14:172-174.
5. Desai MA, Gedde SJ, Feuer WJ, Shi W, Chen PP, Parrish RK, 2nd. Practice preferences for glaucoma surgery: a survey of the American Glaucoma Society in 2008. *Ophthalmic Surg Lasers Imaging* 2011;42:202-208.
6. Gedde SJ, Herndon LW, Brandt JD, Budenz DL, Feuer WJ, Schiffman JC. Postoperative complications in the Tube Versus Trabeculectomy (TVT) study during five years of follow-up. *Am J Ophthalmol* 2012;153:804-814 e801.
7. Gedde SJ, Schiffman JC, Feuer WJ, Herndon LW, Brandt JD, Budenz DL. Three-year follow-up of the tube versus trabeculectomy study. *Am J Ophthalmol* 2009;148:670-684.
8. Kee C. Prevention of early postoperative hypotony by partial ligation of silicone tube in Ahmed glaucoma valve implantation. *J Glaucoma* 2001;10:466-469.
9. Schwartz KS, Lee RK, Gedde SJ. Glaucoma drainage implants: a critical comparison of types. *Curr Opin Ophthalmol* 2006;17:181-189.
10. Villamarin A, Roy, S, Bigler, S, Stergiopoulos, N. A new adjustable glaucoma drainage device. *Invest Ophthalmol Vis Sci* 2014.
11. Stergiopoulos N. Non-invasively adjustable drainage device. *US Patent* 2011;12:743-955.
12. Bigler S. SN. Apparatus and methods for treating excess intraocular fluid. *US Patent* 2012;13:349-353.
13. Dahan E, Carmichael TR. Implantation of a miniature glaucoma device under a scleral flap. *J Glaucoma* 2005;14:98-102.
14. Bouhenni RA, Dunmire J, Sewell A, Edward DP. Animal models of glaucoma. *J Biomed Biotechnol* 2012;2012:692609.
15. Werner L, Chew J, Mamalis N. Experimental evaluation of ophthalmic devices and solutions using rabbit models. *Vet Ophthalmol* 2006;9:281-291.
16. Samsel PA, Kisiswa L, Erichsen JT, Cross SD, Morgan JE. A novel method for the induction of experimental glaucoma using magnetic microspheres. *Invest Ophthalmol Vis Sci* 2011;52:1671-1675.
17. Ruiz-Ederra J, Verkman AS. Mouse model of sustained elevation in intraocular pressure produced by episcleral vein occlusion. *Exp Eye Res* 2006;82:879-884.
18. Shareef SR, Garcia-Valenzuela E, Salierno A, Walsh J, Sharma SC. Chronic ocular hypertension following episcleral venous occlusion in rats. *Exp Eye Res* 1995;61:379-382.
19. de Jong LA. The Ex-PRESS glaucoma shunt versus trabeculectomy in open-angle glaucoma: a prospective randomized study. *Adv Ther* 2009;26:336-345.

20. Nyska A, Glovinsky Y, Belkin M, Epstein Y. Biocompatibility of the Ex-PRESS miniature glaucoma drainage implant. *J Glaucoma* 2003;12:275-280.

Chapter 5 : 4th Paper

Published in IOVS, May 2012.

Eye vessel compliance as a function of intraocular and arterial pressure and eye compliance

Villamarin Adan¹, MSc., Roy Sylvain^{1,2}, M.D., Ph.D., Stergiopoulos Nikolaos¹, Ph.D.

¹Swiss Federal Institute of Technology, Lausanne, Switzerland, ²Glaucoma Center Montchoisi Clinic, Lausanne, Switzerland

Invest. Ophthalmol. Vis. Sci. May 14, 2012 vol. 53 no. 6 2831-2836

Doi: 10.1167/iops.11-8752

Submitted: October 6, 2011.

Accepted: March 21, 2012

5.1 Introduction

Age-related macular degeneration (AMD) is a leading cause¹ of blindness in industrialized countries. However, the causes of this complex disease are not yet well understood. Genetics² and other risk factors, such as smoking, hypertension or elevated cholesterol,^{3,4} have been identified to have a role in the development of such disease. Among other causes, vascular factors also have been hypothesized to contribute to the onset of AMD pathophysiology.^{5,6} Retinal imaging technologies, such as color Doppler imaging,⁷ laser Doppler flowmetry,⁸ and angiographic techniques,⁹ have shown abnormalities in the choroidal circulation by revealing reduced flow velocities and increased resistance indices in the central retinal artery of AMD patients. Several studies have reported that changes in ocular blood flow or in ocular vessel diameter can affect highly the development of the disease. Results of these studies support the hypothesis of an increase in choroidal vascular resistance due to a decrease in the ocular compliance.^{5,10} From that perspective, other studies demonstrated that the pulsatile amplitude of the blood flow pulse in retinal arteries was higher in the presence of AMD.^{11,12} Patients with AMD would likely have a stiffer, less compliant arterial vasculature feeding the eye, as a result of age-related degenerative changes in collagen and elastin.¹³ Furthermore, the elastin layer composing the Brunch's membrane at the level of the macula, and the walls of large arteries analyzed in patients suffering from AMD was found to be thinner and more porous than that in controls.¹⁴ These observations would reinforce the relationship between AMD and the stiffening of systemic vessels. Consequently, it seems that there probably should be a relationship between some cardiovascular diseases affected by low arterial compliance and AMD.

Therefore, it is of interest to develop methodologies for noninvasive or minimally invasive monitoring of the compliance of the eye vessels, as this may prove useful in diagnosing retinal diseases, such as AMD. The purpose of our study was to develop and test a new methodology to assess the compliance of the eye vessels based on physiological parameters and biomechanical properties of the eye, specifically the intraocular pressure (IOP), arterial pressure, and ocular rigidity of the eyeball.

5.2 Materials and Methods

5.2.1 Mathematical model

The model developed in this study is based on the pressure-volume relationship of the eye and the ocular arteries. Volume compliance is defined by $C = \Delta V / \Delta P$ where ΔV is the change in volume for a given change in pressure (ΔP). Equation (1), below, defines the compliance for the arterial network (subscript a) and the eye (subscript e), respectively. C_e , in particular, defines the compliance of the entire eyeball, (combination of sclera and cornea).

$$C_a = \frac{\Delta V_a}{\Delta P_a} \quad \text{and} \quad C_e = \frac{\Delta V_e}{\Delta P_e} \quad (1)$$

During the heart cycle, pulsatile imbalances of blood into and out of the eye lead to changes in the volume of blood within the ocular space. Similarly, imbalances in aqueous production and aqueous outflow may create volume fluctuations, but in the short time scale of a single heartbeat such imbalances in the production and outflow of aqueous humor are assumed to be negligible. Hence, the variation in ocular volume during the heart beat is identical to blood volume variation, so that

$$\Delta V_a = \Delta V_e \quad (2)$$

These volume variations are related to changes in arterial and ocular pressure via their corresponding volume compliances:

$$\begin{aligned} \Delta V_a &= C_a \Delta P_a \\ \Delta V_e &= C_e \Delta P_e \end{aligned} \quad (3)$$

From eqs (2) and (3) we obtain the following simple relation between changes in volume of the heartbeat and the volume compliances of eye and ocular vascular bed

$$C_a \Delta P_a = C_e \Delta P_e \quad (4)$$

which permits the estimation of intraocular vascular bed compliance C_a based on estimated of eye compliance C_e and measurements of intraocular and arterial pressure variations.

$$C_a = C_e \frac{\Delta P_e}{\Delta P_a} \quad (5)$$

5.2.2 *In vitro study*

Six freshly enucleated eyes (post-mortem time less than 4h) from white New Zealand rabbits were obtained from a local farm. The eye was held on a brace and the anterior chamber was canulated with a 24G catheter (Optiva® W, Smiths Medical, Rossendale, UK) filled with a saline solution. The catheter was placed between the anterior plane of the iris and the inner surface of the cornea. This perfusion set-up was connected to an electronic pressure transducer (BLPR2, World Precision Instruments, FL, USA) by a stopcock to measure the IOP corresponding to ΔP_e (eq. 1).

A 3F Fogarty artery embolectomy catheter balloon (Fogarty®, Edwards Lifesciences™, CA, USA) was used to induce volume changes within the eye, mimicking the volume changes of the vascular network of the eye during a heartbeat. The catheter was inserted in the posterior chamber and connected to a microsyringe pump (SP210iw, World Precision Instruments, FL, USA) filled of a saline solution. The volume of the balloon was changed periodically and at a rate of 1-2 Hz producing variations in intraocular volume in the range of 10 to 20 μ l. These variations in volume correspond to ΔV_a in eq. 1 and are accompanied by changes in pressure (ΔP_a , eq.1) in a range of 150 to 350 mmHg.

The perfusion set-up was connected to a data acquisition card (DAQPad-6015, National Instruments, TX, USA) that collected and displayed the signals using a custom made LabView interface (National Instruments, TX, USA). The IOP and balloon pressure were measured in this experiment, whereas the compliance of the eyeball (C_e , eq.1) was determined

in a companion experiment as described below. The compliance of the balloon (representing the compliance of the vascular network of the eye, C_a , eq. 1) was estimated experimentally based on relation (5) using data of IOP, balloon pressure and compliance of the eyeball (this method was defined as *the indirectly measured compliance*). The indirectly measured balloon compliance was compared to balloon compliance estimated directly from pressure-volume obtained from the differential volume injected in the balloon and the corresponding change in intra-balloon pressure (Figure 5-1).

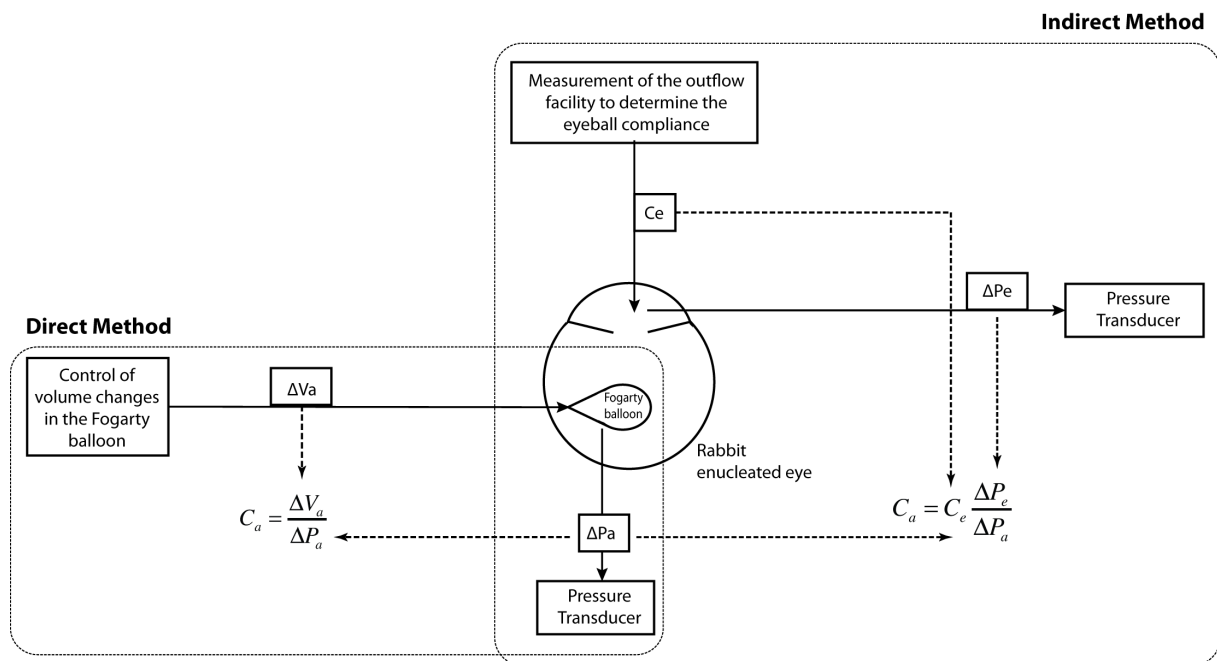


Figure 5-1: Estimation of the compliance of the Fogarty balloon. In the direct method, the volume of the balloon was changed periodically (ΔV_a) and the resulting pressure (ΔP_a) was measured with a pressure transducer. In the indirect method, changes of ΔV_a produced variations in intraocular volume (ΔV_e) resulting in changes in intraocular pressure (ΔP_e). The compliance of the eyeball (C_e) was determined with a companion experiment involving the measurement of the outflow facility.

5.2.3 Eyeball compliance

The eyeball compliance was calculated from outflow facility using the method described by Pallikaris et al¹⁷. In brief, the IOP was artificially increased and recorded from 10 to 25 mmHg using a micropump at a rate of 100 $\mu\text{l}/\text{min}$. The net volume into the eye was estimated by subtracting outflow from inflow, the outflow being estimated from the outflow facility, as explained in the following paragraph. The eye compliance was then determined as the ratio of

the net volume of the eye and the increase in IOP. For calculation individual-specific eyeball compliance was used.

The outflow facility is used to determine the eyeball compliance in both the *in vitro* and *in vivo* experiments. Details of outflow facility measurement have been previously reported^{15, 16}. Briefly, the anterior chamber was perfused at first with a defined flow rate (2 µl/min). After a stable IOP level was reached, the flow rate was changed to a higher value until another stable IOP level was reached. The value of the change in flow rate divided by the IOP change measured represents the outflow facility (*OF*). The outflow facility is thus calculated using the Goldman equation

$$OF = \Delta Q / \Delta IOP \quad (\Delta Q = (Q_2 - Q_1)) \quad (6)$$

where Q_1 and Q_2 are successive inflow rates (µl/min), $\Delta IOP = (P_2 - P_1)$, where P_1 and P_2 represent IOP at Q_1 and Q_2 respectively (mmHg).

In vivo study

Five white New Zealand rabbits (3.5-4.5 kg) were used for this study. General anesthesia was performed using a mixture of a 3 mg/kg (body mass) Xylazine and a 35 mg/kg Ketamin intramuscular injection. Under general anesthesia, the central ear artery was cannulated using a 24G catheter (Optiva® W, Smith Medical, Rossendale, UK) and a 1 French Gauge diameter intra-arterial pressure guide (ComboWire®, Volcano, CA, USA) was inserted through the 24G catheter. Systolic, diastolic and blood pressures were measured using the intra-arterial pressure guide at a rate of 100 Hz and the arterial pulse pressure amplitude was measured taking the diastolic-systolic pressure difference. The pressure sensor was located at about 10 cm from the heart.

Using the same type of Optiva® W catheter the anterior chamber of the eye was cannulated to measure the IOP after the lids were kept open using a wired lid speculum. The catheter was

connected to a pressure sensor (BLPR2, World Precision Instruments, FL, USA). Intraocular pressure was kept in the range of 10 to 25 mmHg to be close to physiological pressure values. Mean arterial pressure and IOP amplitude were acquired to establish baseline conditions. Then, Norepinephrine (10 µg/bolus) was administered intra arterially and the mean arterial pressure and IOP amplitude were acquired. The eyeball compliance was determined before and after norepinephrine injection. The compliance of the vascular network of the eye was calculated using the IOP amplitude, the pulse pressure amplitude and the eyeball compliance before and after norepinephrine injection. After acquiring data on one eye, the second eye was cannulated the same way and the same experimental procedure was followed. At the end of the experimentation the animal was sacrificed with a 120 mg/kg Pentobarbital intra arterial injection. All the experiments conformed to the ARVO Statement for the Use of Animals in Ophthalmic and Vision Research and were reviewed and approved by the institutional committee for animal studies in Lausanne, Switzerland.

5.2.4 Statistics

The results were expressed as the mean and standard deviation (mean ± SD). The paired Student's t-test was used to assess significant differences and effects of norepinephrine administration on the results. $P < 0.05$ was considered statistically significant.

5.3 Results

5.3.1 In vitro study

The outflow facility was 0.35 ± 0.07 µl/mmHg·min and the compliance of the eyeball was equal to 14.13 ± 4.03 µl/mmHg (Table 5-1).

Table 5-1: Summary of the In Vitro Fogarty Balloon Compliance Measurements

Enucleated Eye #	Ocular Compliance of the Eyeball ($\mu\text{L}/\text{mm Hg}$)	Fogarty Balloon Compliance		
		Indirect Method (equation 5, $\mu\text{L}/\text{mm Hg}$)	Direct Method (from pressure-volume curve, equation 1, $\mu\text{L}/\text{mm Hg}$)	Difference
1	18.1	0.062 ± 0.009	0.06 ± 0.005	3.3%
2	13.35	0.059 ± 0.011	0.058 ± 0.007	2%
3	20.06	0.096 ± 0.019	0.105 ± 0.015	-9%
4	11.12	0.088 ± 0.016	0.091 ± 0.009	-2.7%
5	12.05	0.086 ± 0.015	0.091 ± 0.009	-4.9%
6	10.11	0.06 ± 0.01	0.058 ± 0.005	3.7%
Mean \pm SD	14.13 ± 4.03	0.075 ± 0.015	0.077 ± 0.02	4.2%

Variations in pressure of the Fogarty balloon, from 150 ± 10 mmHg to 350 ± 37 mmHg resulted in IOP variation from 0.6 ± 0.1 mmHg to 3.2 ± 0.4 mmHg.

Results of the estimation of compliance of the Fogarty balloon using both direct and indirect methods are depicted in Table 5-1. Direct and indirect estimates of balloon compliance were 0.075 ± 0.017 and 0.077 ± 0.021 $\mu\text{L}/\text{mmHg}$, respectively. The mean ratio between the directly and indirectly measured compliances was 0.99 ± 0.05 , suggesting there is no significant difference between the two methods ($p = 0.86$) (Figure 5-2).

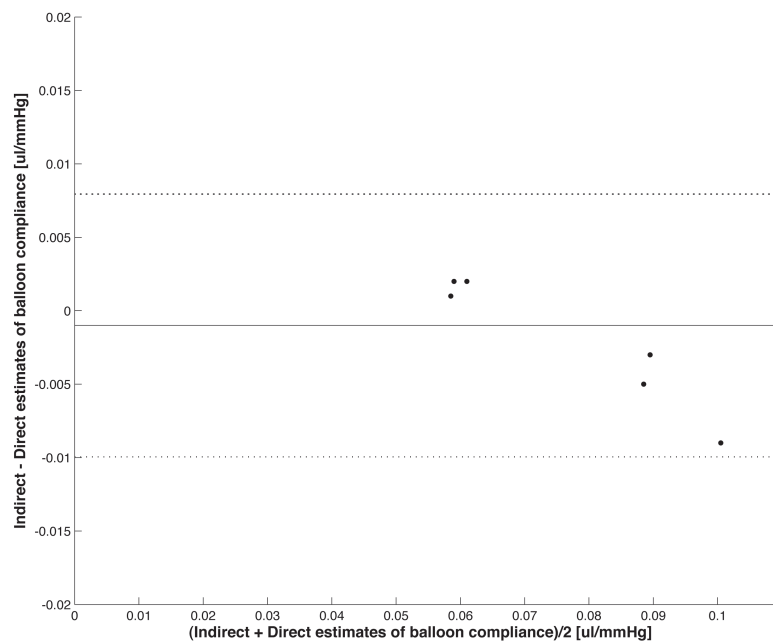


Figure 5-2: Compliance of the Fogarty balloon. Bland-Altman graph comparing the indirect and direct estimates of balloon compliance.

5.3.2 *In vivo study*

The mean outflow facility of the 10 rabbit eyes was equal to $0.209 \pm 0.09 \mu\text{l}/\text{mmHg}\cdot\text{min}$. Norepinephrine increased the mean arterial pressure by 70%, an effect that was highly significant compared to the baseline ($p < 0.001$) (figure 5-3A). As expected this increase in mean arterial pressure was accompanied by 60% increase ($p < 0.001$) in arterial pulse pressure amplitude (figure 5-3B). The mean ocular pulse pressure amplitude (IOP pulse) increased after NE administration from $1.21 \text{ mmHg} (\pm 0.24)$ to $1.55 \text{ mmHg} (\pm 0.2)$ ($p < 0.05$, figure 5-3C). Finally, the arterial compliance significantly decreased after administration of NE from $0.18 \mu\text{l}/\text{mmHg} (\pm 0.12)$ to $0.10 \mu\text{l}/\text{mmHg} (\pm 0.08)$ ($p < 0.05$, figure 5-3D).

Eye compliance was significantly reduced after NE injection ($p < 0.05$) with compliance being equal to $4.07 \pm 1.49 \mu\text{l}/\text{mmHg}$ and $2.93 \pm 1.48 \mu\text{l}/\text{mmHg}$ before and after injection, respectively (figure 5-3E).

5.4 *Discussion*

We have developed a new method to predict the compliance of the vascular network of the eye. Based on the principle of continuity and the variations of IOP and arterial pressure over the cardiac cycle, we have derived a simple relation which gives the compliance of the vascular network of the eye, C_a , as the product of eyeball compliance, C_e , times the ratio of IOP variation over arterial pulse pressure ($\Delta P_e/\Delta P_a$). The eyeball compliance was characterized in a parallel experiment following the outflow facility measurements.

An *in vitro* approach, where a Fogarty catheter with a compliant balloon simulating the compliance of the ocular vessels was inserted in enucleated rabbit eyes, was used to validate the proposed model. The experiment showed that inflation of the Fogarty catheter induced an increase of the IOP. The results showed that the compliance of the Fogarty catheter balloon

can be predicted using our formula (Eq 5) quite precisely, with the average error being statistically insignificant and always less than $\pm 5\%$ (Table 5-1).

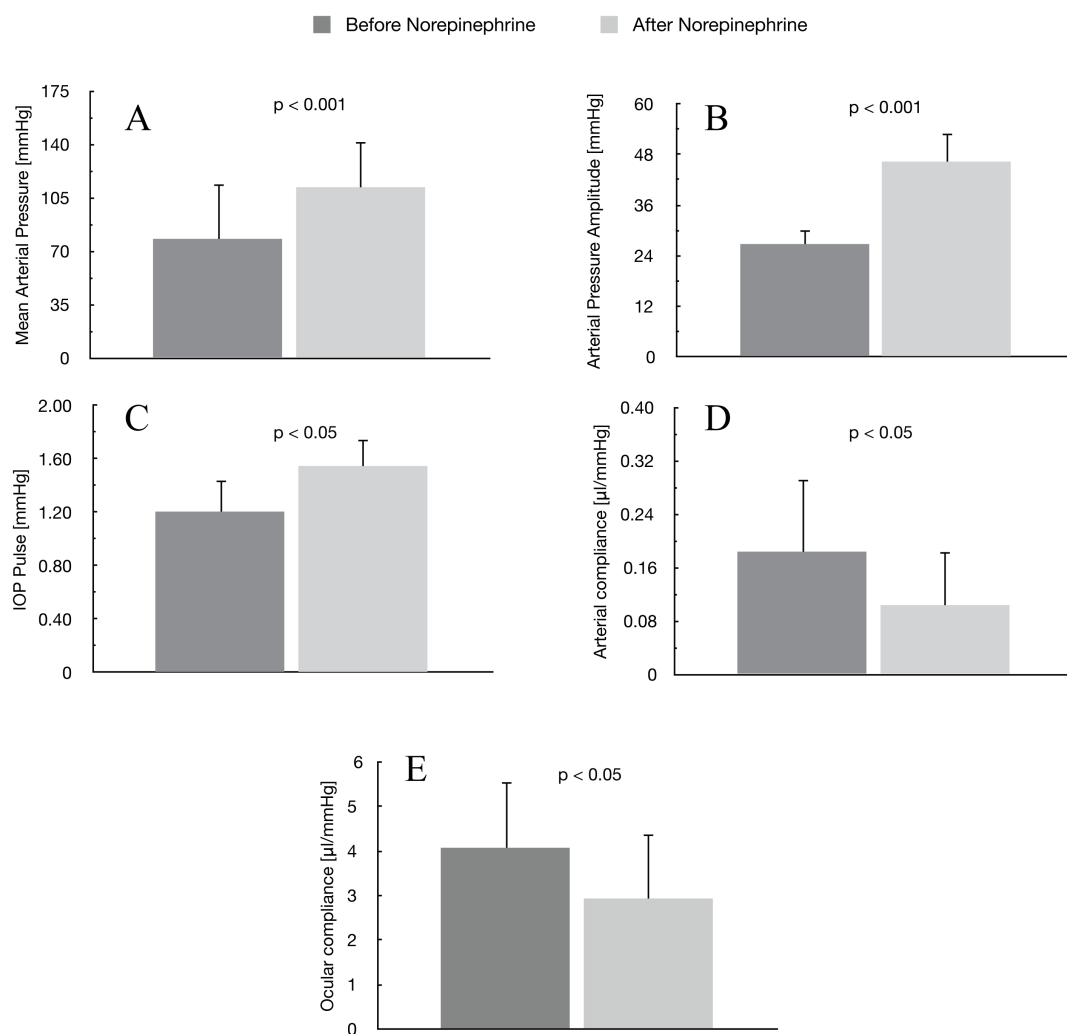


Figure 5-3: Effects of norepinephrine on the arterial pressure amplitude (A), mean arterial pressure (B), IOP pulse (C), arterial compliance (D), and ocular compliance (E). Data are presented as means and SD values. P values are calculated from paired t-tests comparing baseline data with data after administration of norepinephrine.

After validating the model *in vitro*, we performed animal experiments to determine the compliance of the vascular system of the eye under control conditions and after administration of norepinephrine. Norepinephrine is a hormone that causes strong arterial vasoconstriction¹⁸. Consequently, the mean arterial pressure and arterial pressure amplitude have increased significantly, as expected¹⁹. According to the results obtained in this study, the arterial compliance has significantly decreased meaning that elevation of the systemic blood pressure changed the effective elastic properties of the arterial system. These findings are

plausible, as we expect that contraction of vascular smooth muscles (VSM) and increase in pressure would lead to decrease in vascular compliance²⁰.

Ocular compliance is a physical parameter of the eye that expresses the elastic properties of the eyeball upon inflation²¹. Based on observations by Langham et al.²², the coefficient of ocular compliance reflects the elastic properties of the sclera and the cornea in cadaveric eyes, where no blood circulation prevails. In contrast, when measured *in vivo* on animal models, ocular rigidity seems to be affected by ocular blood volume. In our study, the coefficient of ocular compliance was higher in enucleated eyes (14.13 $\mu\text{l}/\text{mmHg}$) compared to living eyes (4.07 $\mu\text{l}/\text{mmHg}$). We postulate that the blood circulation and the resulting vascular tone could have possibly contributed to the observed increase in the eye rigidity. It is worth mentioning that the ocular compliance, C_e , which is needed to calculate the intraocular vascular compliance, cannot be obtained noninvasively. Our *in vivo* measurement of the pressure-volume relation of the rabbit eyeball were in accordance with the results presented by Kymionis et al.²³, who evaluated the ocular rigidity of 16 rabbit eyes after photorefractive keratectomy. Dastiridou et al.²⁴ studied the pressure-volume relation in the living human eye and found that the pulsatile change in IOP is directly related to the rigidity of the ocular layers that dampen the pulsations. The latter suggests that higher ocular pulse amplitude may be found in eyes with increased rigidity, due to either a higher rigidity coefficient or a higher IOP. In our study administration of NE increased the coefficient of ocular rigidity raising the ocular pulse pressure amplitude. This observation consolidates the statement made by Dastiridou and colleagues.

Results from *in vivo* experiments have shown that NE significantly altered not only the compliance of the vascular network in the eye, C_a , but also the elastic properties of the eyeball, C_e . This could possibly suggest that decrease in compliance of ocular vessels leads to a more rigid and less compliant eyeball. Previous studies have shown that both ocular and vascular

compliance of the eye are affected by retinal disease. Friedman and associates¹⁰ have suggested that ocular rigidity plays a role in the development of AMD. They stated that the coefficient of scleral rigidity of age-related macular degeneration patients was higher than that of controls meaning that a more rigid sclera would likely alter compliance of vessels embedded in a less compliant surrounding. Later Pallikaris et al.²⁵ also measured the ocular rigidity in patients suffering from AMD, distinguishing between the different types of AMD. Their results draw conclusions comparable to Friedman as they showed that the eye rigidity data were significantly higher in presence of neovascular AMD in comparison with the non-neovascular form and the group of control patients. Sato et al.^{11, 12} stated that patients with AMD have a less compliant arterial network in the eye. They showed that the pulse wave velocity and the pressure associated with the central aortic blood pressure waveform were higher in patients with AMD compared to controls¹² implying that an increase in vascular rigidity would lead to a stiffer scleral wall. All these findings suggest that AMD may be associated with increased vascular and eye rigidity. As stated before Friedman and Pallikaris suggested that an increasingly rigid sclera would affect the arterial compliance, encapsulating the ocular vasculature in a less compliant compartment. However, in our study we have demonstrated that a deliberate increase in the systemic arterial rigidity resulted in a corresponding elevation of the eye rigidity (Figure 5-3E). Consequently, we could suggest that a stiffer ocular arterial network could result in stiffer eyeballs. We may further add that the parameter C_a (arterial compliance) should be considered as a component of the overall eyeball compliance C_e . That is, C_a reflects not only the compliance of the vessel branches within the posterior chamber, but also incorporates the choroidal vasculature and intra-scleral vasculature. Hence, modifying the stiffness of this extended vasculature would necessarily impact overall eyeball stiffness, as they are inter-related. When considering previous studies on age-related macular degeneration and eyeball rigidity, a question remains unresolved: are the AMD-related haemodynamic abnormalities the result of an increase in the scleral rigidity,

or would elevation of the systemic vascular stiffness lead to further scleral rigidity? Further studies are needed to clarify this question.

In conclusion, we have proposed a method to estimate the compliance of the ocular vascular network, based on measurements of eyeball compliance, IOP and arterial pressure. The stiffness of the arterial network in the eye may be an important factor in the initiation and development of retinal disease. Age-related macular degeneration is a good example of how abnormalities in elastic properties of the choroidal blood vessels can alter the structure of the retina and ultimately the sight. Further studies should include human subjects to assess the link between changes in ocular vascular network compliance to retinal disease such as AMD.

5.5 Acknowledgments

We are grateful to the staff from Hôpitaux Universitaires de Genève (HUG) and Mr. Reda Hasballa for their contribution to this study.

5.6 References

1. Tomany SC, Wang JJ, Van Leeuwen R, et al. Risk factors for incident age-related macular degeneration: pooled findings from 3 continents. *Ophthalmology* 2004;111:1280-1287.
2. Klein ML, Mauldin WM, Stoumbos VD. Heredity and age-related macular degeneration. Observations in monozygotic twins. *Arch Ophthalmol* 1994;112:932-937.
3. Seddon JM, Rosner B, Sperduto RD, et al. Dietary fat and risk for advanced age-related macular degeneration. *Arch Ophthalmol* 2001;119:1191-1199.
4. Smith W, Assink J, Klein R, et al. Risk factors for age-related macular degeneration: Pooled findings from three continents. *Ophthalmology* 2001;108:697-704.
5. Friedman E. A hemodynamic model of the pathogenesis of age-related macular degeneration. *Am J Ophthalmol* 1997;124:677-682.
6. Friedman E. The role of the atherosclerotic process in the pathogenesis of age-related macular degeneration. *Am J Ophthalmol* 2000;130:658-663.
7. Friedman E, Krupsky S, Lane AM, et al. Ocular blood flow velocity in age-related macular degeneration. *Ophthalmology* 1995;102:640-646.
8. Pournaras CJ, Logean E, Riva CE, et al. Regulation of subfoveal choroidal blood flow in age-related macular degeneration. *Invest Ophthalmol Vis Sci* 2006;47:1581-1586.
9. Axer-Siegel R, Bourla D, Priel E, Yassur Y, Weinberger D. Angiographic and flow patterns of retinal choroidal anastomoses in age-related macular degeneration with occult choroidal neovascularization. *Ophthalmology* 2002;109:1726-1736.
10. Friedman E, Ivry M, Ebert E, Glynn R, Gragoudas E, Seddon J. Increased scleral rigidity and age-related macular degeneration. *Ophthalmology* 1989;96:104-108.
11. Sato E, Feke GT, Menke MN, Wallace McMeel J. Retinal haemodynamics in patients with age-related macular degeneration. *Eye (Lond)* 2006;20:697-702.
12. Sato E, Feke GT, Appelbaum EY, Menke MN, Trempe CL, McMeel JW. Association between systemic arterial stiffness and age-related macular degeneration. *Graefes Arch Clin Exp Ophthalmol* 2006;244:963-971.
13. Klein R, Klein BE, Tomany SC, Cruickshanks KJ. The association of cardiovascular disease with the long-term incidence of age-related maculopathy: the Beaver Dam Eye Study. *Ophthalmology* 2003;110:1273-1280.
14. Chong NH, Keonin J, Luthert PJ, et al. Decreased thickness and integrity of the macular elastic layer of Bruch's membrane correspond to the distribution of lesions associated with age-related macular degeneration. *Am J Pathol* 2005;166:241-251.
15. Nguyen C, Boldea RC, Roy S, Shaarawy T, Uffer S, Mermoud A. Outflow mechanisms after deep sclerectomy with two different designs of collagen implant in an animal model. *Graefes Arch Clin Exp Ophthalmol* 2006;244:1659-1667.
16. Delarive T, Rossier A, Rossier S, Ravinet E, Shaarawy T, Mermoud A. Aqueous dynamic and histological findings after deep sclerectomy with collagen implant in an animal model. *Br J Ophthalmol* 2003;87:1340-1344.
17. Pallikaris IG, Kymionis GD, Ginis HS, Kounis GA, Tsilimbaris MK. Ocular rigidity in living human eyes. *Invest Ophthalmol Vis Sci* 2005;46:409-414.
18. Cobbold AF, Lewis OJ. The action of adrenaline, noradrenaline and acetylcholine on blood flow through joints. *J Physiol* 1956;133:472-474.

19. Bartter FC, Mills IH, Gann DS. Increase in aldosterone secretion by carotid artery constriction in the dog and its prevention by thyrocarotid arterial junction denervation. *J Clin Invest* 1960;39:1330-1336.
20. Dobrin PB, Rovick AA. Influence of vascular smooth muscle on contractile mechanics and elasticity of arteries. *Am J Physiol* 1969;217:1644-1651.
21. Friedenwald JS. Contribution to the theory and practice of tonometry. *Am J Ophthalmol* 1937;20:985-1024.
22. Langham ME, Farrell RA, O'Brien V, Silver DM, Schilder P. Blood flow in the human eye. *Acta Ophthalmol Suppl* 1989;191:9-13.
23. Kymionis GD, Diakonis VF, Kounis G, et al. Ocular rigidity evaluation after photorefractive keratectomy: an experimental study. *J Refract Surg* 2008;24:173-177.
24. Dastiridou AI, Ginis HS, De Brouwere D, Tsilimbaris MK, Pallikaris IG. Ocular rigidity, ocular pulse amplitude, and pulsatile ocular blood flow: the effect of intraocular pressure. *Invest Ophthalmol Vis Sci* 2009;50:5718-5722.
25. Pallikaris IG, Kymionis GD, Ginis HS, Kounis GA, Christodoulakis E, Tsilimbaris MK. Ocular rigidity in patients with age-related macular degeneration. *Am J Ophthalmol* 2006;141:611-615.

Chapter 6 : Conclusion

The lack of IOP control over time remains one of the main problems in the management of glaucoma. Many of the complications related to glaucoma filtering surgery are linked to a lack of prediction of the IOP level achieved and maintained. Motivated by the drawbacks of the current procedures and devices used in glaucoma filtering surgery as well as their complications, a new non-invasively adjustable glaucoma drainage device has been developed. This implant aims at providing a viable solution to current glaucoma drainage devices adding an additional feature, which is an adjustable flow resistor. In that prospect, the purpose is to minimize the early post-operative hypotony and to control the evolution of the IOP by selectively changing the resistance to aqueous humor outflow.

Hypotony is a common problem found in all glaucoma filtering procedures, often leading to further complications. The implant developed in this thesis aims at reducing the risk of post-operative hypotony by increasing the resistance to aqueous outflow in the early post-operative stages. Thanks to its internal mechanism, the AGDD allows changes in the cross-sectional area of a draining tube, and thus adjustment in the resistance to flow. Considering the progressive nature of the scarring tissue and the wound healing response after implantation, it is anticipated that the 'valve' should be set at a relatively closed position during the early post-operative period to be progressively opened later on, maintaining optimal IOP level during the entire postoperative period.

The different tests conducted during this study have demonstrated the efficacy and the ease of use of the AGDD through in vitro and in vivo experiments. The adjustability of the device has been shown to be reproducible, however the range of adjustment between the functional fully open position to the fully closed position offers a rather small range of manageability (approximately 50 degrees or 4 to 5 functional positions). The range of adjustment has to be increased in order to offer a larger operational range for the clinicians. The procedure of implantation has demonstrated some similarities to conventional filtering surgeries such as the implantation of the Ex-PRESS® or even trabeculectomy. This kind of surgery is comparable to standard procedures performed by eye surgeons.

Extensive series of tests (biocompatibility, sterility, bioburden, etc.) according to applicable regulatory standards have been carried out successfully, allowing for the CE marking of the device and validating the safety of the device for human implantation. Naturally, the materials used for the assembly of the AGDD are certified as biocompatible and safe for human use. However, further investigations still need to be conducted on humans to assess the safety, performance and efficacy of the device, especially at the long-term.

In this thesis the AGDD has been always described as a stand-alone device. Nonetheless, the design of the implant offers some innovative options, e.g. the connection to a seton tube has been foreseen for further draining possibilities. That way the drainage of the aqueous humor does not occur under the sclera next to the limbus, but takes place rather far under the subconjunctival in the equatorial region of the eyeball. Fibrous response should therefore develop on a much less extent as compared to what prevails closer to the limbus, thus enhancing the rate of success. In addition, the connection could even be extended to a further point, reaching the orbit of the eye, where fibrosis formation would be minimal.

Perspectives

The next objective for the AGDD is the performance of human clinical trials. Safety, performance and efficacy will be tested, providing a refined answer on the clinical benefits and advantages that the implant may offer. Future clinical trials should not only test the device itself but also the kind of procedure used for the implantation. We may thus assert whether the AGDD could be placed as a stand-alone device or in combination with a seton tube. Both procedures should be carefully tested in order to enlarge the field of application of the AGDD.

Curriculum Vitae

Adan VILLAMARIN

Av. de la Gare 19d
1022 Chavannes-près-Renens, VD
078/675.24.91
adan.villamarin@epfl.ch
Spanish
26.01.1985
Married

- Engineer in **Bioengineering/Biotechnology**
- Interest in **Medtech** industry
- **Team spirit, analytical and practical abilities, motivated.**

Education

2009 – 2014	PhD in the Doctoral Program of Biotechnology and Bioengineering at EPFL <ul style="list-style-type: none">• PhD Thesis : « Development and testing of a new non-invasively adjustable glaucoma drainage device »
2007 – 2009	Master studies in Bioengineering/Biotechnology at Ecole Polytechnique Fédérale de Lausanne (EPFL) <ul style="list-style-type: none">• Master project: “<i>Evaluation of a telemetrically operated and controlled glaucoma drainage device.</i>”• <i>Focus on Biophysics, Fluid Mechanics & Management of Technology</i>
2003 – 2007	Bachelor in Life Sciences at EPFL <ul style="list-style-type: none">• <i>Bachelor Project: “Motif discovery in conserved non-coding regions of the genome.”</i><ul style="list-style-type: none">○ <i>Focus on Perl programming, use of DNA databases</i>
2000 – 2003	Maturité Fédérale with emphasis in Mathematics/Physics and complementary option in Economics, <i>Beaulieu, Lausanne</i>

Experiences

2008 - 2009	Assistant/Student – Laboratory for Mechanobiology & Morphogenesis, Prof. Swartz Goal: <i>Analyze and process cell-tracking movies. Process of Excel tables with Matlab</i> <ul style="list-style-type: none">• Software: Axiovision, Metamorph, Imaris & Matlab.
Summer 2006	Internship at Institut Suisse de Recherche Expérimentale sur le Cancer (ISREC) in Pr. Grapin-Bottom’s group Subject: <i>Study of pancreatic cells expressing pdx1 during early stages of embryogenesis</i> <ul style="list-style-type: none">• Developmental and Molecular biology, microscopy.
2002 – 2007	Work experience Mauerhofer & Zuber electrical corporation as an <u>electrical fitter</u> <ul style="list-style-type: none">• Prototype design, machine assembly and microchip set-up.

Skills

Computer

Excellent knowledge of MS-Office tools (Word, Excel, PowerPoint, Access, etc.)

Knowledge in Perl – C++ programming

Labview – Matlab – Solidworks – Photoshop – Illustrator – Blender

Languages

French Mother tongue

Spanish Mother tongue

English Fluent (C1 - CEFR)

Extra-scholar activities

From 2013

President of Vo-Vietnam Crissier, Vietnamese traditional martial art

- Organization of international workshops and demonstration

2007 – 2009

President of the Junior Entreprise EPFL

- Leadership of a team of 15 members
- Management and supervision of more than 30 consulting projects
- Established key partnerships with companies

Hobbies

Ski, Martial Arts, Mountain bike

Scientific Publications and Meetings

Publications:

- Villamarin et al. A new adjustable glaucoma drainage device. *IOVS*. March 25, 2014 vol. 55 no. 3 1848-1852
- Villamarin et al. 3D simulation of the aqueous flow in the human eye. *Med Eng Phys*. Dec, 2012 vol. 34 no. 10 1462-1470
- Villamarin et al. Eye vessel compliance as a function of intraocular and arterial pressure and eye compliance. *IOVS*. May 14, 2012 vol. 53 no. 6 2831-2836

Oral Presentation:

- Villamarin et al. Eye vessel compliance as a function of intraocular and arterial pressure and eye compliance. ASME. 2012, Puerto Rico

References

Pr. Stergiopoulos Laboratory of Hemodynamic and Cardiovascular
Technology, EPFL
Dr. Roy Glaucoma Center, Montchoisi Clinic, Lausanne